

# Defining Ventilation Boundary Conditions for a Greenhouse Climate Model

D.E. Dwyer





# **Defining Ventilation Boundary Conditions for a Greenhouse Climate Model**

MASTER THESIS

D.E. Dwyer

August 29, 2014



The work in this thesis was supported by TNO. Their cooperation is hereby gratefully acknowledged.



Copyright ©  
All rights reserved.



---

# Abstract

Presently 10% of natural gas supplied to the Netherlands is used to maintain a stable climate and continuous electricity within horticultural greenhouses. As a result, technologies that reduce this energy consumption are in high demand. Theoretical models of heat flows in greenhouses can be used as a tool to increase the efficiency of these developments. This work seeks to improve such a tool by modeling the effects of various window opening angles and wind directions on the ventilation boundary condition for a greenhouse climate model.

Using OpenFOAM, Computational Fluid Dynamics (CFD) simulations of various window opening angles and wind directions were run for both external and internal flow of a Venlo-type greenhouse. A thorough verification of the simulation results examined spatial convergence, temporal convergence, model implementation, iterative convergence, and consistency. The results of these simulations were deemed insufficient for a boundary analysis due to initial flow field errors. While the variable results could not be applied to a boundary condition analysis, the constant case (with 30 degree window openings and a zero degree azimuth angle) was used to reproduce the internal flow field of the greenhouse.

The resulting model contained concentrated error at windows where fixed velocity values are not prescribed, correcting for continuity. This boundary condition is a first step towards more accurate internal greenhouse flow simulations of ventilation. Further, methods for generating a ventilation boundary condition using verified variable simulation results are discussed for future use.



---

# Table of Contents

<b>Acknowledgements</b>	<b>ix</b>
<b>1 Introduction</b>	<b>1</b>
1-1 Project Motivation . . . . .	1
1-1-1 Current state of the Kasklimaat Model (KKM) . . . . .	2
1-1-2 Future Plans for the Greenhouse Climate Model . . . . .	3
1-2 Project Objectives . . . . .	3
1-3 Thesis Overview . . . . .	4
1-4 Terminology . . . . .	4
<b>2 Theoretical Background</b>	<b>7</b>
2-1 Ventilation . . . . .	7
2-1-1 Wind-Driven Flow . . . . .	7
2-1-2 Buoyancy-Driven Flow . . . . .	8
2-1-3 Combined Effect of Buoyancy and Wind . . . . .	8
2-2 Computational Fluid Dynamics . . . . .	9
2-2-1 Finite Volume Approach . . . . .	9
2-2-2 Numerical Model: Discretization for the Navier-Stokes System . . . . .	10
2-2-3 Turbulence . . . . .	13
<b>3 Methodology</b>	<b>17</b>
3-1 Model Parameters . . . . .	17
3-2 Wind Direction . . . . .	18
3-3 Window Opening Angle . . . . .	18
<b>4 CFD Simulation</b>	<b>21</b>
4-1 Boundary Conditions . . . . .	22
4-2 Numerical Approach . . . . .	23
4-2-1 Solution and Algorithm Control . . . . .	24
4-2-2 Numerical Schemes . . . . .	25
4-3 Simulation Methods . . . . .	26

<b>5 Verification and Validation of Results</b>	<b>27</b>
5-1 Verification . . . . .	27
5-1-1 Examine Spatial Convergence . . . . .	27
5-1-2 Examining Temporal Convergence . . . . .	32
5-1-3 Examine the Implementation of the Model . . . . .	32
5-1-4 Examine Iterative Convergence . . . . .	33
5-1-5 Examine Consistency . . . . .	37
5-2 Validation . . . . .	42
5-3 Results . . . . .	43
<b>6 Boundary Analysis</b>	<b>47</b>
6-1 Selecting parameters . . . . .	47
6-2 Parameter value specification . . . . .	50
6-2-1 Interpolation . . . . .	50
6-2-2 Multiple regression analysis . . . . .	51
<b>7 Recommendations</b>	<b>53</b>
<b>8 Conclusion</b>	<b>55</b>
<b>A Appendix: Boundary Conditions</b>	<b>57</b>
<b>B Appendix: Calculation Details</b>	<b>59</b>
<b>Bibliography</b>	<b>63</b>
<b>Glossary</b>	<b>67</b>
List of Acronyms . . . . .	67
List of Symbols . . . . .	67

---

# List of Figures

1-1 Terminology diagram . . . . .	5
2-1 Staggered grid . . . . .	10
3-1 Wind azimuth angles . . . . .	19
3-2 15 and 30 degree window openings . . . . .	19
3-3 53.3 Degree window opening . . . . .	19
4-1 3-Dimensional greenhouse models . . . . .	22
4-2 Overview of computational domain from the top and side views . . . . .	23
5-1 Top view of larger computational domain . . . . .	28
5-2 Larger Computational Domain Mesh . . . . .	28
5-3 Velocity magnitude flow field in large computational domain . . . . .	28
5-4 Velocity magnitude flow field in computational domain . . . . .	29
5-5 Top view of finely meshed grid . . . . .	29
5-6 Side view of finely meshed grid with twice as many cells in each dimension . . . . .	30
5-7 Spatial Convergence Study . . . . .	31
5-8 Monitoring of Courant value for each time step . . . . .	32
5-9 Initial residual error for each time step for (a) a zero degree wind approach angle and (b) a 75 degree wind approach angle . . . . .	33
5-10 Temporal fluctuations of the drag coefficient . . . . .	34
5-11 Temporal fluctuations of the drag coefficient . . . . .	35
5-12 Temporal fluctuations of calculated fields for a 0 degree wind approach angle and 30 degree window openings . . . . .	36
5-13 Temporal fluctuations of calculated fields for a 75 degree wind approach angle and 30 degree window openings . . . . .	37
5-14 Comparison between initial and final velocity magnitude at the window openings . . . . .	39
5-15 Comparison between initial and final pressure at the window openings . . . . .	39
5-16 Volumetric flow rate at windows for varied window opening angle calculations . . . . .	40
5-17 Vector plot of velocity for a slice located along the leeward facing windows in a simulation containing closed windward facing windows . . . . .	40

5-18 Velocity boundary condition [ $m/s$ ] . . . . .	41
5-20 x component of velocity field . . . . .	43
5-21 Results for y component of velocity field . . . . .	44
5-22 Results for z component of velocity field . . . . .	44
5-23 Velocity vector field at a plane parallel to the ground located (a) 1 meter from the ground and (b) 3.7 meters from the ground, colored by velocity magnitude . . . . .	44
5-24 Volumetric flow rate at windows of the 'constant' case . . . . .	45
5-25 Pressure field of the 'constant' simulation . . . . .	46
5-26 Results for turbulent kinetic energy field . . . . .	46
5-27 Results for turbulent kinetic energy dissipation field . . . . .	46
6-1 Selecting boundary condition parameters . . . . .	49
6-2 Selecting boundary condition parameters: effect on pressure distribution . . . . .	49
6-3 Selecting boundary condition parameters: Effect on velocity distribution . . . . .	50

---

# List of Tables

4-1	Atmospheric Boundary Layer (ABL) Conditions . . . . .	24
4-2	Residual error tolerances used in the Pressure Implicit with Splitting of Operators (PISO) algorithm for each parameter . . . . .	25
4-3	Numerical Schemes . . . . .	25
5-1	Spatial convergence details . . . . .	30
5-2	Percentage of stationary window probes in varied wind azimuth angle calculations (with fixed 30 degree windward and leeward window opening angles) . . . . .	38
5-3	Percentage of stationary window probes in simulations of varied window opening angle combinations (with fixed 0 degree wind approach angle) . . . . .	38
A-1	Boundary conditions . . . . .	58



---

# Acknowledgements

These past two years in the Netherlands have brought many memories and learning experiences that I am grateful for. In particular, the past nine months of thesis work would not have been possible without the help and support of many people. I would like to thank my industry supervisors Ivo Kalkman and Leonard Baart de la Faille for their time and patience working with me over the past 9 months. Additionally, thanks to my TU Delft supervisors Rene Delfos and Mathieu Pourquie.

Besides my academic support, my time in the Netherlands would not have been the same without my friends and roommates, who showed me the bright side of Delft. Finally, without the encouragement and support of my family I never would have considered moving to the Netherlands.

Delft, University of Technology  
August 29, 2014

D.E. Dwyer



---

# Chapter 1

---

## Introduction

The highest concentration of greenhouses in the world is located in the Netherlands. Greenhouses can provide controlled crop growth, shelter from external climate conditions, and protection from pest invasions. Therefore, the Dutch greenhouses enable the country to take the lead as the largest exporter of tomatoes in the world [1]. With their expertise in glass greenhouse technology, the Dutch are also the largest exporter of greenhouse equipment [2]. Hence, Netherlands Organization for Applied Scientific Research (TNO)'s greenhouse research and development initiatives have followed suit, spanning 40 years of greenhouse knowledge creation. The focus of their work has targeted increased access to sunlight and reduced energy consumption.

Within the industry, it is commonly known that greenhouses are a major consumer of energy, maintaining their warm temperatures and powering their electricity needs with 10% of the natural gas supplied to the Netherlands. The latest technologies that have been developed to address this issue include screens that retain heat within different layers of height in the greenhouse, external screens to increase exterior insulation of the greenhouse, and dehumidification systems that minimize heat loss. Furthermore, an evenly distributed climate can increase crop productivity. In order to test the impact of new technologies such as these, theoretical models of heat flows can increase the efficiency of these developments.

Computational fluid dynamics is a powerful tool for simulating internal greenhouse climate. It is used because of its wide range of applicability in comparison to simpler models, which come with limitations. Extensive research on greenhouse Computational Fluid Dynamics (CFD) modeling has already been done: Between the years 2000 and 2012, 214 papers and 88 articles were published about CFD modeling of greenhouses [3]. Developing an accurate CFD solver, however, can be very complicated, and is not always a field of knowledge that is familiar to the engineers developing energy efficient greenhouse technologies.

### 1-1 Project Motivation

As a result, TNO has set out to develop a Kasklimaat Model (KKM), which translates in English to Greenhouse Climate Model. While a multitude of scientists have developed greenhouse models that predict thermal flows, humidity control, and carbon dioxide exchanges, what makes this model unique is the ultimate end-use goals. The model will be distributed as an easy-to-use greenhouse climate modeling software. Possible uses for this technology can include development of greenhouse regulations, testing new technological developments for greenhouses, and testing new greenhouse

designs. The second use for this model would be for model-based control. The conditions inside the greenhouse (i.e. temperature, humidity, and carbon dioxide levels) must be very precise for optimal plant growth. However, in such a large space, physical effects like buoyancy and wind can cause gradients in greenhouse parameters to occur, requiring control systems for adjustment.

In order to meet these two goals, the ultimate product must use numerical methods and simplifications to accurately calculate the physical conditions inside the greenhouse at a fast rate. The parameters modeled in the KKM are density, pressure, temperature, gas composition, flow velocity, radiation intensity (both solar and heat), and turbulence. Components included in the model are heaters, fans, screen fabric, and windows. A major challenge in developing this model is predicting the internal flows without modeling the entire external environment.

### 1-1-1 Current state of the KKM

Although TNO has been modeling greenhouse climate for nearly two years, the development of the latest KKM has been underway since June, 2013. The project began with an initial review of the physical parameters that must be included in the model in order to accurately and realistically model a greenhouse. A review of existing greenhouse climate models was also completed, to avoid redundancy. Next, a simplified 3D CFD model was implemented in MATLAB. The model was then transitioned to OpenFOAM in order speed up the calculation time and further develop the model while making optimal use of the functionality that was already available.

Both transient and steady-state preliminary greenhouse solvers have been developed in OpenFOAM. The steady-state model is necessary in order to initialize the simulation prior to the transient solver. It can also be used when the user has no interest in dynamical processes but merely in the situation which will develop after sufficient time has passed. The model runtime has been optimized using local time stepping methods for model based control applications. There is still progress to be made within each of the following physical parameters.

- The temperature parameter currently accounts for buoyancy, wall heat transfer (by indicating an outside temperature and thermal conductivity), heat radiation (considered as a constant or direction dependent emissivity), and heater sources (specified on boundaries or within the volume). Planned improvements on this parameter include incorporating specific heater power per volume, implementing the effect of obstacles on radiation view factors, and adding the effect of solar radiation heat transfer.
- The gas composition parameter accounts for component gases (with variable compositions), water condensation on cold surfaces (using the Colburn-Hougen equation), and evaporation (as a constant). The calculation of this parameter will be improved by changing the evaporation rate to depend on other variables, validating the condensation model, and incorporating sources and sinks for non-water components.
- The flow velocity parameter accounts for buoyancy-driven flow, the effect of porous media, and the effect of fans as either a pressure difference or outflow velocity. This parameter will be improved by coupling the flow and temperature of porous media, defining fans and screens independently of the mesh, and including turbulence effects of flow through porous media and past fans. At the beginning of this project, the effect of flow around windows, and the effect of external wind flow on internal velocities was not yet included.
- The radiation intensity parameter currently accounts for heat radiation, and will eventually incorporate solar radiation into the calculation.

Beyond the physical parameters, the model will be tested and validated using existing greenhouse measurements and tests in an experimental greenhouse facility.

Lattice Boltzmann computing techniques are also under consideration as a possible alternative to conventional CFD methods. Rather than modeling fluxes over control volumes, as simulated using CFD, Lattice Boltzmann simulations model the fluid as a series of propagations and collisions of particles. This method is known for its computational efficiency, eliminating the need to explicitly solve pressure dynamics. It is considered a robust method for large scale simulations.

### 1-1-2 Future Plans for the Greenhouse Climate Model

The plan for the KKM in 2014 is to improve the model by incorporating the missing physical elements, improving the speed of the calculation, and testing Lattice Boltzmann computing techniques. Moving in the direction of the ultimate product goal, the model will also be expanded to include parameters that are greenhouse specific, installation specific, crop specific and location specific. Finally, the model will be validated using greenhouse measurements and controlled experiments in a local experimental greenhouse to prove that it is consistent with reality.

Given the current state and future plans for the KKM project, the flow velocity parameter was deemed a critical component for the model, and was selected as the focus for this work. Analyzing the effect of external climatic conditions on the internal greenhouse climate can ultimately lead to the development of more efficient designs and enhanced ventilation management. At the start of this project, there were two calculation methods missing from the model that rely on external flow conditions: external air exchanges resulting from flow around windows and from pressure differences caused by external flows.

## 1-2 Project Objectives

Ventilation in greenhouses is driven by both buoyancy and wind. While stack-driven ventilation can be modeled relatively accurately without the need for CFD, using zonal modeling, it is the air exchanges that occur near the window that are less predictable. Eddies near windows can cause an outflow containing the same air carried into the greenhouse, rather than allowing the greenhouse to exchange air with the external environment. While numerous studies have investigated the effects of external flows on the overall ventilation rate of greenhouses, there is still a lack of information detailing how external flow conditions may be used to characterize the flow field at the ventilation boundary. This aspect of the KKM can most greatly benefit from CFD modeling.

The research question defining this graduation project is

*Can CFD be used to define a realistic boundary condition at the window openings of an interior greenhouse climate model to represent the effect of external wind?*

The conditions this study accounts for are wind direction, wind speed, window opening angle, and greenhouse geometry. The following procedure is used to address this research question and arrive at the end results:

- Complete an initial literature review of relevant existing research
- Model a greenhouse with varying external environments to be used as a basis for determining boundary condition trends

- Validate models using available measurements
- Analyze results of various external (and resulting internal) environments and deduct a methodology for prescribing these trends on an enclosed greenhouse model
- Prescribe unique boundary conditions at the windows in the interior KKM, which only models the greenhouse interior, and compare the results with the validated external models

### 1-3 Thesis Overview

This report is organized with the following structure:

- The thesis begins with an overview of the theoretical background in Chapter 2, covering both the driving forces behind greenhouse ventilation and a discussion of the CFD algorithm used in this work.
- Chapter 3 goes into detail about the methods used to select and test variables that can be used to derive a greenhouse ventilation boundary condition.
- The computational methods for calculating the effects of different variables are discussed in detail in Chapter 4. This section discusses both the mesh generation, boundary conditions, and numerical schemes used to stabilize the calculation.
- Chapter 5 provides a discussion of the convergence of the resulting simulations, an overview of the flow behavior within the greenhouse, and a validation of the results using available experimental data.
- In Chapter 6, methods for formulating and implementing a ventilation boundary conditions using the external flow simulations are discussed.
- Chapter 7 provides recommendations for further work and improvements,
- followed by concluding remarks in Chapter 8.

### 1-4 Terminology

Beyond the abbreviations and symbols provided in the appendix of this report, there is some basic horticultural greenhouse terminology that is used throughout this work that must be identified for the reader.

Horticultural greenhouses with glass coverings are often made up of repeated long narrow segments with either an A-shaped or arched roof. The term *span* refers to one of these segments. *Ridges* are the peak of the span roof and *gutters* are the valleys between two spans. These values are identified in Figure 1-1.

Windows are sometimes referred to as *ventilators*. Along an A-shaped roof, windows are differentiated by the direction they face. Windows located upwind of the roof ridge are *windward-facing*, while windows downwind of the roof ridge are *leeward-facing*. The *opening angle* of the window commonly discussed in this work is an angle (in degrees) measured from the plane of the roof surface to the window flap, with the ridge as the vertex. Examples of three different window opening angles are depicted in Figures 3-2 and 3-3.

The angle at which the wind approaches the greenhouse is called the *wind azimuth angle*. A wind azimuth angle of zero is perpendicular to the ridges of the greenhouse. The angle is measured

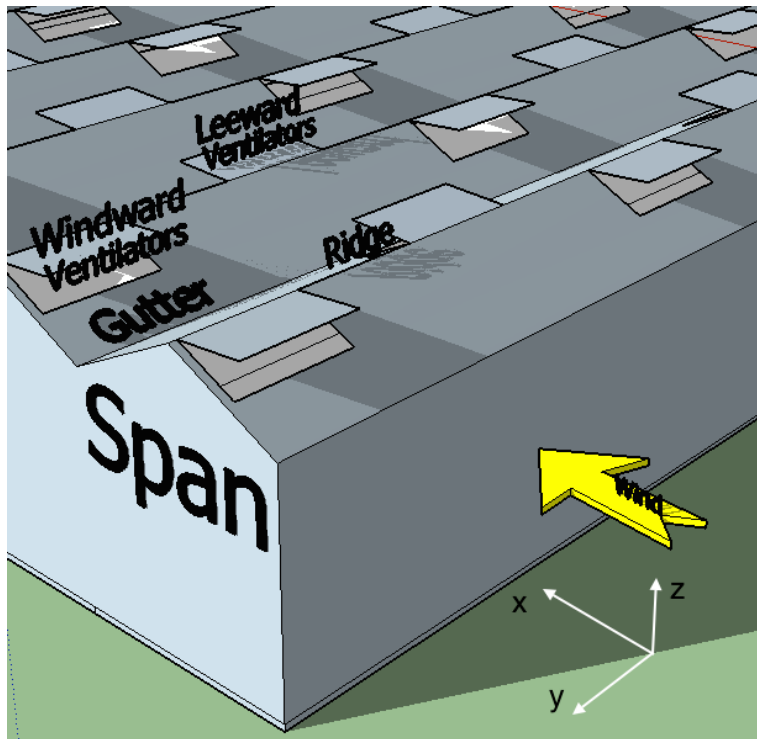


**Figure 1-1:** Terminology

counterclockwise from the zero degree wind azimuth angle. Figure 3-1 provides a visualization for this concept.

Sometimes, references are made to the position of a window within the greenhouse. *Span number* identifies the span where the window is located, with the first span located upwind, and the last span located downwind. Span number increases in the stream-wise direction. On an x, y, z coordinate system, the origin is located at the most upwind point of the greenhouse, along the ground on the far right-hand corner (as observed from upwind). The x-axis is perpendicular to the ridges of the greenhouse, the y-axis is oriented parallel to the ridge, and the z-axis is representative of the greenhouse height.



---

# Chapter 2

---

## Theoretical Background

This chapter presents the relevant theory used to calculate the greenhouse ventilation boundary condition. It begins with an overview of the driving forces that cause ventilation, and continues with the numerical methods used to compute this behavior.

### 2-1 Ventilation

Ventilation air exchanges result from temperature and pressure differences between the inside and surroundings of a greenhouse. Crop production in greenhouses is most greatly influenced by ventilation efficiency [4]. This is because ventilation enhances parameters that effect crop development and production: it removes excessive heat within the greenhouse; enhances carbon dioxide and oxygen exchanges; maintains acceptable humidity levels [5]; and manages biotic transfers such as fungal spores [6]. Ventilation has a seasonal function, reducing excess humidity during the winter and cooling the greenhouse interior during the summer.

Greenhouse ventilation can be naturally or mechanically driven. While mechanical ventilation is driven by electric fans, natural ventilation through windows is driven by both wind and buoyancy forces. Natural ventilation is generally more cost effective, and is therefore the more widely used ventilation method. However, sensitivity analyses show that external factors like wind speed, wind direction, and temperature can greatly influence natural ventilation rates [7].

Ventilation is most commonly described in terms of pressure differences. The wind force causes pressure differences near the windows, while a gradient in air density between the inside and outside result in a vertical pressure gradient which drives the buoyancy force (also known as the stack effect). Natural ventilation is dominated by the wind force at velocities greater than 2 m/s [8] [9], and by the buoyancy force in the winter, when temperature differences are greater between the interior and exterior of the greenhouse.

#### 2-1-1 Wind-Driven Flow

Wind-driven ventilation occurs when air interacts with an obstacle, generating a pressure distribution around the greenhouse. Pressure drops at the windows can be related to velocity through a window opening, as described by Bernoulli's equation (assuming that air is incompressible):

$$\Delta P_w = \frac{1}{2} \rho C_p U^2 \quad (2-1)$$

where  $\Delta P_w$  is the pressure drop due to wind,  $U$  is wind speed,  $\rho$  is the air density, and  $C_p$  is the non-dimensional pressure coefficient. The pressure coefficient is defined as

$$C_p = \frac{P - P_0}{\frac{1}{2} \rho U_0^2} \quad (2-2)$$

where  $P$  is the static pressure at some point in the flow,  $P_0$  is the static pressure at the undisturbed stream,  $U_0$  is the velocity of the undisturbed stream.

## 2-1-2 Buoyancy-Driven Flow

Temperature differences between the building interior and exterior, or within spaces in a building cause buoyancy forces, thereby driving the airflow. For the case of buoyancy-driven flow, the Boussinesq approximation is used to determine the pressure difference,  $\Delta P_s$  which drives airflow through a window opening. This method assumes incompressible flow, and homogeneous temperature distributions in- and outside the window.

$$\Delta P_s(y) = \Delta P_0 - \rho g \frac{\Delta T}{T} z \quad (2-3)$$

where  $\Delta P_0$  is the pressure at ground level,  $T$  is the outside temperature,  $\Delta T$  is the temperature difference between the inside and outside,  $\rho$  is density, and  $z$  is the vertical coordinate.

## 2-1-3 Combined Effect of Buoyancy and Wind

The weight of buoyancy force compared to wind force is expressed with the dimensionless Richardson,  $Ri$ , (or Archimedes) number  $Ri = \frac{g'h}{u^2}$ , where  $g'$  represents reduced gravitational acceleration,  $g' = \frac{\Delta \rho}{\rho_0}$ , and  $u$  represents the wind speed. Gravitational acceleration is applied for Boussinesq approximations, when density differences in the fluid are low. A Richardson number less than unity indicates that the flow is dominated by the wind force, while a Richardson number much greater than unity indicates dominance of buoyancy force. However, the less dominant force cannot be ignored. Mistriotis et al. observed significant effects of buoyancy forces despite the dominance of wind forces [10].

The combined effect of buoyancy and wind for greenhouse ventilation calculations has been studied in detail by Boulard and Baille [11], concluding that the model that best fits experimental measurements calculates ventilation from the sum of the two pressure differences.

$$\Delta P = \Delta P_s + \Delta P_w \quad (2-4)$$

The resulting velocity through the windows is related to this pressure drop by

$$\Delta P = \frac{1}{2} \rho \zeta U^2 \quad (2-5)$$

where  $\zeta$  is a pressure drop coefficient.

## 2-2 Computational Fluid Dynamics

Several methods are used to study the behavior of greenhouse climate due to ventilation. Until recently, field experiments have been the predominant method, using techniques such as impulse peak and continuous injection tracer gas tests to visualize the behavior; and sonic anemometry and thermocouples to quantify air velocity and temperature. However, these techniques require many sensors in order to provide an accurate description of velocity, temperature, and humidity patterns. Wind tunnel tests have also been a popular experimental method, providing more control over the external wind conditions [12]. While theoretical ventilation can be simply calculated assuming perfect mixing, Computational Fluid Dynamics (CFD) makes it possible to model the turbulence, complex flow patterns, and temperature and humidity distributions that occur within the greenhouse, resulting in varied crop quality.

This method eliminates the need for costly facilities and equipment. Furthermore, several studies have compared experimental methods to CFD, finding results qualitatively in agreement with wind tunnel tests and field measurements. However, evidence from literature shows that CFD studies of greenhouses tend to differ quantitatively, generating results that deviate between 16.3 and 44% from experimental measurements [13], [4], [14], [15].

CFD, a method in which flow equations are solved numerically, has become a commonly used method for calculating ventilation patterns for the purpose of evaluating ventilation efficiency [16]. An iterative process is used to apply the conservation equations to each control volume and calculate model variables. Both wind- and stack-driven ventilation can be modeled using CFD.

### 2-2-1 Finite Volume Approach

The discretization method used for this work divides the computational domain into finite volumes, where the center of each domain defines the solution. In contrast to the finite element and finite difference methods, the finite volume method utilizes the integral form of the conservation equations to calculate the fluxes at the surfaces of each finite control volume. An advantage of this method in comparison to the finite difference method is that conservation can be enforced as long as the surface integral is consistent along adjacent boarders. The sum of all control volume surface fluxes results in the global conservation, because internal surface fluxes cancel out. While second order calculations are generally accepted to be an accurate calculation method, higher order methods (above second order) are more difficult to achieve with the finite volume approach [17].

#### Staggered Grid

The finite volume method begins with discretizing the computational domain. Given the complex pressure-velocity coupling discussed in the following section, it is common to use a staggered grid, in which scalar variables (pressure, in this case) are defined at ordinary nodal points, while velocity components are calculated on staggered grids centered at cell faces [18]. If velocities and pressures are both defined at the same node, then a oscillating non-uniform pressure field can act like a uniform field (in instances where oscillations are present). The staggered grid method eliminates the need to interpolate velocity at the cell faces for the transport calculations. It also allows pressure differences at adjacent nodes to act as the driving force for velocity. A depiction of the 2-dimensional staggered grid is seen in Figure 2-1. The  $u$ -velocities are stored at  $e$  and  $w$  cell faces, while the  $v$ -velocities are stored at  $n$  and  $s$  cell faces.

In this staggered arrangement, the pressure gradient term,  $\frac{\partial p}{\partial x}$ , for example, can be calculated with

$$\frac{\partial p}{\partial x} = \frac{p_P - p_W}{\delta x_u} \quad (2-6)$$

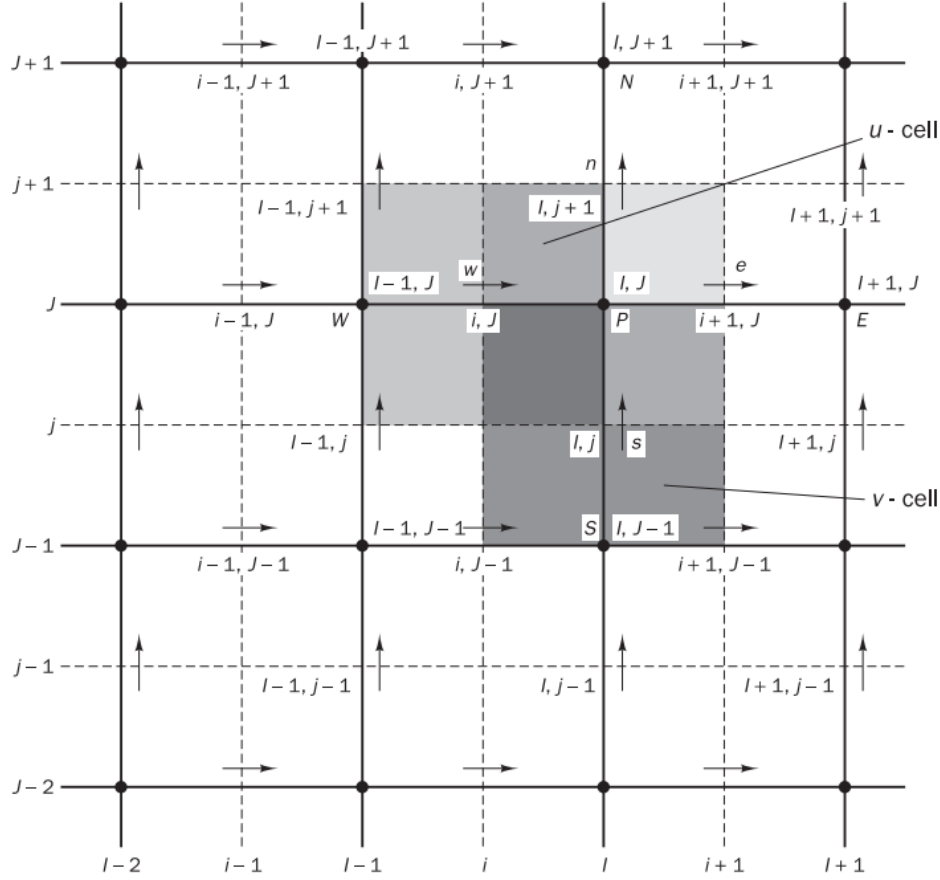


**Figure 2-1:** 2-dimensional staggered grid used for coupled pressure-velocity systems. Pressure is stored at nodes marked ( $\bullet$ ) and velocity is defined at the cell faces, marked with arrows (horizontal arrows ( $\rightarrow$ ) indicate  $u$ -velocities and vertical arrows ( $\uparrow$ ) indicate  $v$ -velocities) [18]

### Rhie-Chow Interpolation

While the staggered grid is very beneficial, it does not translate well to unstructured meshes, and could result in unphysical pressure oscillations. The OpenFOAM CFD software makes use of an interpolation method closely related to the Rhie-Chow interpolation method [19], which satisfies the need for discretized calculations on unstructured grids. Rhie-Chow interpolation is used for the discretization of the transport equation, and is elaborated on in the derivation of the pressure equation in the following section.

The method involves interpolating discretized variables by introducing a coefficient for pressure-velocity coupling. The interpolation can be seen as a correction proportional to the difference between the pressure gradient at the face and the interpolated pressure gradient at the face [20].

### 2-2-2 Numerical Model: Discretization for the Navier-Stokes System

The calculation method used to evaluate the effect of wind assumes air to be an incompressible fluid, due to the fact that pressure does not vary greatly within the model. With a nearly zero mach number,  $M = \frac{u}{u_{sound}} \approx 0$ , density is independent of dynamic pressure. Incompressible fluids can be described using the following general conservation equation:

$$\frac{\partial \varphi}{\partial t} + \frac{\partial(U\varphi)}{\partial x} + \frac{\partial(V\varphi)}{\partial y} + \frac{\partial(W\varphi)}{\partial z} = \Gamma_\varphi \nabla^2 \varphi + S_\varphi \quad (2-7)$$

where  $\varphi$  represents the non-dimensional form of the transported quantity;  $U$ ,  $V$ , and  $W$  are the three velocity vector components;  $\Gamma_\varphi$  is the diffusion coefficient; and  $S_\varphi$  is the source term. In words, the transport equation can be stated as:

$$\text{rate of increase of } \varphi + \text{net flow rate of } \varphi \text{ out of the control volume} = \text{rate of increase of } \varphi \text{ due to diffusion} + \text{rate of increase of } \varphi \text{ due to sources}$$

CFD flow solvers use a set of coupled Partial Differential Equations (PDEs) to iteratively calculate flow variables for each control volume. The unsteady nature of flow within greenhouses requires the use of an incompressible, transient flow solver to model the various external situations imposed on the greenhouse model. The momentum equation can be derived from the general transport equation for incompressible flow (Eq 2-7) by replacing  $\varphi$  with the velocity vector,  $u$ .

#### *Momentum equation*

$$\frac{\partial u}{\partial t} + \nabla \cdot (uu) - \nabla \cdot (\nu \nabla u) = -\nabla p \quad (2-8)$$

#### *Continuity equation*

$$\nabla \cdot u = 0 \quad (2-9)$$

For the greenhouse case considered, three momentum equations exist (one for each velocity component), and all three velocity components are present in the continuity equation. The purely incompressible system eliminates coupling between density and pressure, in addition to coupling between energy and the rest of the system.

The solver used in this work makes use of the Pressure Implicit with Splitting of Operators (PISO) algorithm, proposed by Issa [21], to solve the incompressible continuity and momentum equations with pressure-velocity coupling. The idea behind the PISO algorithm is to use multiple pressure corrections to solve the two complex coupling terms present in the pressure-velocity systems:

- a non-linear convection term with  $u$ - $u$  coupling
- intricate linear pressure-velocity coupling (due to all three velocity components appearing in each momentum equation and the continuity equation), making it challenging to solve for pressure.

### **Solving Non-Linearity**

The non-linear convection term represents the transport of velocity. An iterative cycle is used to solve for the non-linear convection term,

$$\nabla \cdot (uu) \approx \nabla \cdot (u^o u^n) \quad (2-10)$$

where  $u^o$  is the current solution and  $u^n$  is the new solution for each iteration, repeating the calculation until  $u^o = u^n$  [22] [18]. While iterative calculations can increase computational cost for large time steps, a small time step can produce a more accurate temporal solution.

### **Deriving the pressure equation**

Coupling between pressure and velocity introduces a constraint on the solution. With no pressure equation for incompressible flow, an equation can be derived from the continuity and momentum equations. The momentum equation is discretized for the velocity at location (P) as

$$a_P^u u_P + \sum_N a_N^u u_N = r - \nabla p \quad (2-11)$$

where  $r = \frac{u^o}{\Delta t}$  is the momentum source term. The momentum equation has been divided through by volume to allow for interpolation of the coefficients at faces. The summation of the north south, east, and west neighbors ( $N$ ) is defined as  $\sum_N a_N^u u_N$ . A  $H(u)$  operator containing both the transport and source terms,

$$H(u) = r - \sum_N a_N^u u_N \quad (2-12)$$

simplifies the equation, to isolate  $u_P$ .

$$a_P^u = H(u) - \nabla p \quad (2-13)$$

$$u_P = (a_P^u)^{-1}(H(u) - \nabla p) \quad (2-14)$$

Substitution of the incompressible continuity equation ( $\nabla \cdot u = 0$ ) results in a pressure equation for incompressible flow [22]

$$\nabla \cdot [(a_P^u)^{-1} \nabla p] = \nabla \cdot [(a_P^u)^{-1} H(u)] \quad (2-15)$$

The pressure gradient is not discretized to conform with the Rhie-Chow interpolation procedure. Interpolation of the  $H(u)$  operator and  $\nabla p$  based on  $a_P^u$  is the essence of Rhie-Chow interpolation.

## Deriving the Face Flux Equation

The conservative face fluxes are corrected before each pressure-corrector step. This section derives the calculation for the face flux,  $F$ . Beginning with the discretized continuity equation,

$$\nabla \cdot u = \sum_f s_f \cdot u = \sum_f F \quad (2-16)$$

where the face flux is the surface normal of the velocity,  $F = s_f \cdot u$ . Substituting velocity from Equation 2-14, the face flux becomes

$$F = s_f \frac{1}{a_P^u} (H(u) - \nabla p) \quad (2-17)$$

Satisfying this equation guarantees face fluxes to be conservative.

## Sequence of Operations

The PISO algorithm uses a segregated guess-and-correct method to solve a sequence of equations.

The first pressure corrector establishes a velocity field, while the following corrector(s) determine the pressure distribution.

The PISO algorithm uses the following method:

1. Momentum predictor: Solve the discretized momentum equation (Eq 2-11) to compute an intermediate velocity field, using the conservative fluxes in Equation 2-17, and pressure,  $p$ , from the previous time step

```

fvVectorMatrix UEqn
(
    fvm::ddt(U)
    + fvm::div(phi, U)
    - fvm::laplacian(nu, U)
);

solve(UEqn == -fvc::grad(p));

```

2. Compute the mass fluxes at the cells faces by interpolation, using an approximate velocity corresponding to  $(a_P^u)^{-1}H(u)$
3. Pressure solution: Solve the pressure equation using the  $H(u)$  operator from the predicted velocities.

```

fvScalarMatrix pEqn
(
    fvm::laplacian(rAU, p) == fvc::div(phi)
);

```

where  $rAU$  corresponds to  $(a_P^u)^{-1}$ .

4. Correct the mass fluxes at the cell faces with 2-17
5. Explicit velocity correction: Correct the velocities using the new pressure field with Equation 2-14.
6. Update the boundary conditions
7. Repeat from 3 for the prescribed number of non-orthogonal corrector steps
8. Increase the time step and repeat from 1[22][23]

### 2-2-3 Turbulence

Instabilities from non-linear inertial and viscous terms in the Navier-Stokes equations result in turbulent flow. Given the rotational nature, vortex stretching is required to maintain the constantly fluctuating vorticity. With vortex stretching absent from 2-dimensional flows, turbulence must be modeled in the 3-dimensional domain. Turbulence is also time-dependent, requiring statistical averaging techniques to estimate fluctuations.

Turbulent eddies are unsteady vortices. The largest eddies are a result of energy from the mean velocity, called turbulent kinetic energy. The energy is passed on to smaller eddies, and eventually dissipated into heat. The scale of the smallest eddies are called the Kolmogorov scales, consisting of length, velocity, and time. Resolving these very small quantities would require a decent amount of computational power. For complex problems with high Reynolds numbers, new variables that approximate these small turbulence quantities are introduced into the equations of motion. The addition of these variables results in an under-defined system of equations. Closure models are used to describe assumed correlations within the equations of motion.

## RANS Methodology

The three commonly used methods for turbulence modeling are Direct Numerical Simulation (DNS), Large Eddy Simulation (LES), and Reynolds Averaged Navier-Stokes (RANS) modeling. RANS turbulence modeling determines time-averaged flow parameters with turbulence modeling. DNS numerically solves the Navier-Stokes equations along with the entire spatial and temporal scales of turbulence without the use of a turbulence model. Memory storage for this method can be very high, in addition to the slow integration over time, requiring a small enough time step to satisfy a Courant number below 1. LES separates fluid movement into large and small eddies, calculating the large eddies in three dimensions, with time dependence, and calculating small eddies on a subgrid scale.

This study is limited to the most widely used, RANS methodology, due to computational memory and speed limitations. This method involves Reynolds decomposition of pressure and velocity coupled with time-averaging of these equations. The Reynolds decomposition breaks down pressure and velocity into a mean and a time-averaged component.

$$u = U + u' \quad (2-18)$$

$$p = P + p' \quad (2-19)$$

This process results in the additional  $-\rho u'_i \bar{u}'_j$  term, known as the Reynolds stress tensor, when applied to the Navier Stokes equation.

The shortened simulation time and reduced memory requirements come with several inaccuracies. Jiang et al. have identified two major problems with the use of RANS for the purpose of calculating both external and internal ventilation flows [24]. The first issue is the inability of RANS to predict airflow around buildings. One study indicates that RANS modeling has difficulty generating the separation region on the roof, and has tendencies to overpredict the recirculation region beyond the bluff body. The second issue observed by Jiang et al. is the modeling of mean flow parameters, with the example of the mean velocity for a single window with uniform flow to be zero, canceling out the air exchanges present in reality. Jiang et al. conclude that RANS is not ideal for modeling ventilation with both the internal and external environment in steady state calculations. However, for the case of large, complex geometries, the method was found to be appropriate, given the necessary computational time and memory for alternatives. For unsteady RANS simulations (used in this work), the problem of overpredicting the recirculation region is less extreme, and the cancelation of air exchanges is not present.

Of the various RANS methodologies, the standard  $k - \epsilon$  model has been commonly used among previous greenhouse ventilation studies [12]. This method solves two additional transport equations: turbulent kinetic energy,  $k$ , and turbulent kinetic energy dissipation,  $\epsilon$  [25]. This model determines eddy viscosity using a single turbulence length scale of motion, assuming turbulent diffusion occurs at a set length scale. There are more accurate alternatives for the situation being modeled that require the same computational capacity. The Re-Normalization Group (RNG) model better predicts detachment and reattachment of flow by introducing modified transport coefficients, accounting for small spatial scales. A more recent model, the realizable  $k - \epsilon$  model, addresses eddy viscosity differently and uses an additional transport equation for the viscous dissipation, which is derived from the vorticity fluctuation transport equation. As a result, this model better represents rotation, flux separations and boundary layers where large pressure gradients occur. The calculations in this work make use of the realizable  $k - \epsilon$  model.

### Realizable $k - \epsilon$ Model

The realizable  $k - \epsilon$  model solves for turbulent kinetic energy and turbulent kinetic energy dissipation using the following simplified transport equations, derived from the mean-square vorticity fluctuations.

$$\frac{\partial}{\partial t}(\rho k) + \frac{\partial}{\partial x_j}(\rho k u_j) = \frac{\partial}{\partial x_j} \left[ \left( \mu + \frac{\mu_t}{\sigma_k} \right) \frac{\partial k}{\partial x_j} \right] + P_k + P_b - \rho \epsilon - Y_M + S_k \quad (2-20)$$

and

$$\frac{\partial}{\partial t}(\rho \epsilon) + \frac{\partial}{\partial x_j}(\rho \epsilon u_j) = \frac{\partial}{\partial x_j} \left[ \left( \mu + \frac{\mu_t}{\sigma_\epsilon} \right) \frac{\partial \epsilon}{\partial x_j} \right] + \rho C_1 S_\epsilon - \rho C_2 \frac{\epsilon^2}{k + \sqrt{\nu \epsilon}} + C_{1\epsilon} \frac{\epsilon}{k} C_{3\epsilon} P_b + S_\epsilon \quad (2-21)$$

where  $P_k$  is the generation of turbulence kinetic energy due to mean velocity gradients ( $P_k = \tau_{ij} \frac{\delta U_i}{\delta x_j}$ ),  $P_b$  is the generation of turbulence kinetic energy due to buoyancy, and  $Y_M$  represents the fluctuating dilation in compressible turbulence that contributes to the total dissipation rate.  $\sigma_k$  and  $\sigma_\epsilon$  are the turbulent Prandtl numbers for the turbulent kinetic energy and its dissipation rate.  $S_k$  and  $S_\epsilon$  are the user-defined source terms.

The turbulent viscosity,  $\mu$ , is dependent on a variable,  $C_\mu$ .

$$\mu_t = \rho C_\mu \frac{k^2}{\epsilon} \quad (2-22)$$

$$C_\mu = \frac{1}{A_0 + A_S \frac{k U^*}{\epsilon}} \quad (2-23)$$

where

$$U^* = \sqrt{S_{ij} S_{ij} + \tilde{\Omega}_{ij} \tilde{\Omega}_{ij}} \quad (2-24)$$

and

$$\tilde{\Omega}_{ij} = \bar{\Omega}_{ij} - 3\epsilon_{ijk}\omega_k \quad (2-25)$$

$\bar{\Omega}_{ij}$  is the mean rate-of-rotation tensor viewed in a rotating reference frame with angular velocity  $\omega_k$ . Constants are defined as  $A_0 = 4.04$  and  $A_S = \sqrt{6} \cos \phi$ , where

$$\phi = \frac{1}{3} \cos^{-1} (\sqrt{6} W) \quad (2-26)$$

$$W = \frac{S_{ij} S_{jk} S_{ki}}{\tilde{S}^3} \quad (2-27)$$

$$\tilde{S} = \sqrt{S_{ij} S_{ij}} \quad (2-28)$$

$$S_{ij} = \frac{1}{2} \left( \frac{\partial u_j}{\partial x_i} + \frac{\partial u_i}{\partial x_j} \right) \quad (2-29)$$

Finally, the  $C$  constants are experimentally determined by Shih et al. as  $C_{1\epsilon} = 1.44$ ,  $C_2 = 1.92$ ,  $C_\mu = 0.09$  [26].



---

# Chapter 3

---

## Methodology

With the goal of modeling the internal conditions of a greenhouse independent of modeling external flows, trends can be derived from simulations of greenhouses with various external environment conditions and geometry configurations. The most important variables relating to external conditions are selected and systematically varied. The calculations of the external greenhouse environment are validated for accuracy using available measurements, before a ventilation boundary condition is deduced from the observed trends. In order to implement the observed ventilation boundary condition trends on an internal greenhouse model, the necessary parameters for running a stable internal greenhouse calculation are determined. The results of the internal models are compared to the calculations containing the full external environment to show that the results reasonably portray the expected flow patterns within the greenhouse.

### 3-1 Model Parameters

Several parameters are selected on the basis of making the model scientifically accurate and providing the appropriate variables for the intended applications. An extensive review of past Computational Fluid Dynamics (CFD) studies on greenhouse ventilation by Bournet and Boulard, 2010 [12], found the following parameters to have varying degrees of impact (organized by driving force).

- buoyancy-driven ventilation
  - temperature difference between inside and outside air
  - differences in relative humidity inside and outside the greenhouse
- wind-driven ventilation
  - wind velocity
  - wind direction
  - window opening angle
  - window direction (leeward vs. windward)
  - span number and greenhouse length
  - window location (distance from windward side)
  - greenhouse height
  - combination of roof and side wall openings
  - presence of nearby buildings

- specific devices such as insect-proof or shading screens, etc.
- greenhouse design
- window size

Due to the time limitations of this work, buoyancy calculations are not included in the analysis. Among the parameters that influence wind-driven ventilation, wind opening angle and wind direction are the primary variables that are investigated. However, the analysis also considers wind velocity.

An empty Venlo-style greenhouse was modeled for this study. The Venlo greenhouse is a pitched roof multi-span greenhouse. The greenhouse is ventilated with 1.2-by-2.2 meter staggered windows along the roof that are open in both the leeward and windward directions. It is made up of 15 greenhouse modules (otherwise known as spans), each 4 meters wide (in the  $x$  direction), 37.5 meters long (in the  $y$  direction), with 5 meter high ridges and 4 meter high gutters (in the  $z$  direction). Details about greenhouse dimensions and terminology, can be found in Figure 1-1. The roof is pitched at 26.7 degrees from the horizontal plane. Furthermore, to prevent water from collecting on the roof, the land the greenhouse sits on is elevated at an inclination of 1.5 mm/m. This is accounted for in the model by placing the greenhouse on a narrow wedge base. While it is ideal to simplify such models for the purpose of CFD calculations, an appropriate number of spans was necessary to observe the reconnecting flow over the roof of the greenhouse. Given the focus on the effect of external conditions on the greenhouse, crops and greenhouse equipment such as screens and heaters were not modeled for this analysis.

The average wind speed was modeled for the Westland region, an area well known for its horticulture and greenhouse industry. Local weather stations belonging to Koninklijk Nederlands Meteorologisch Instituut (KNMI) (in English, the Royal Netherlands Meteorological Institute), indicate an average wind speed of 3.7 m/s at the height of the greenhouse windows [27]. This value is extrapolated from 10-meter high weather station measurements assuming atmospheric boundary layer conditions discussed in Section 4.2 with the relation

$$u_z = \frac{u_{10}}{\ln\left(\frac{10+z_0}{z_0}\right)} \ln\left(\frac{z+z_0}{z_0}\right) \quad (3-1)$$

where  $u_z$  is the velocity at a specified height,  $z$ ,  $u_{10}$  is the weather station velocity measured at a height of 10 meters, and surface roughness length,  $z_0$  is set to 0.1m.

## 3-2 Wind Direction

Wind azimuth angle was varied in 15 degree increments from 0 to 90 degrees, where a 0-degree azimuth angle represents wind perpendicular to the greenhouse ridge, and a 90-degree azimuth angle indicates wind flowing parallel to the ridge. The symmetry of the greenhouse structure can be used to deduce ventilation patterns resulting from approach angles outside the 0 to 90 degree range.

## 3-3 Window Opening Angle

Venlo greenhouses are characterized by alternating (windward- and leeward-facing) discontinuous window openings, which result in complex 3-dimensional flows. It is common for the leeward- and windward-facing windows to be open at different angles. Hence, for this study, combinations of opening angles between 0 and 100% are investigated (0, 15, 30, and 53.3 degree window opening angles). The maximum window angle occurs when the window panel is parallel to the adjacent roof slope. For the roof slope of 26.7 degrees, the maximum ventilation opening occurs at an angle 53.3 degrees from the roof surface.

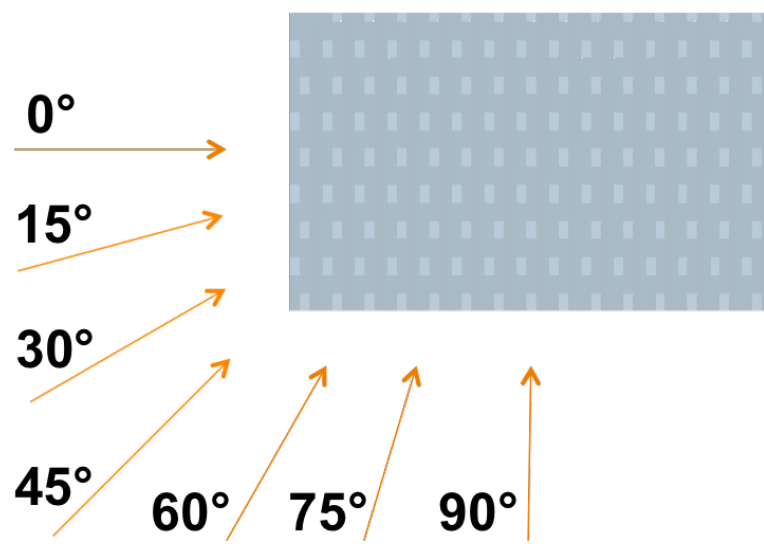


**Figure 3-1:** Wind azimuth angles

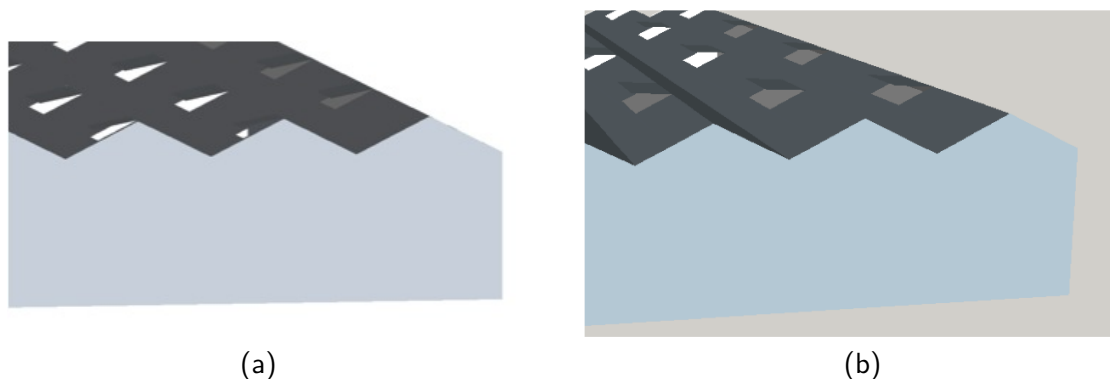


**Figure 3-2:** 15 and 30 degree window openings

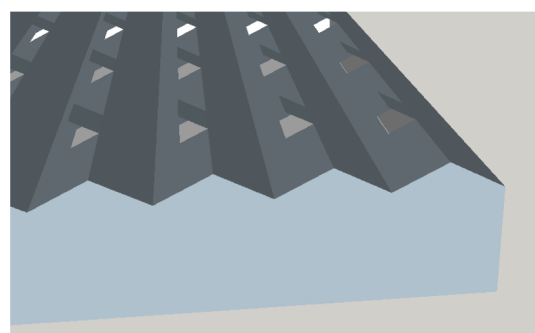


**Figure 3-3:** 53.3 degree window opening angle



---

# Chapter 4

---

## CFD Simulation

This section discusses the approach used to develop the meshes, calculate flow patterns, and simulate the various external conditions.

OpenFOAM is a powerful Computational Fluid Dynamics (CFD) tool that was selected on the conditions that it is efficient, extensive, and as an open source software package, it is easily modifiable, flexible, and has no licensing costs. Working with OpenFOAM also presents several drawbacks: integrating the software with optimization methods and experiments can be a challenge, and as an open source software licensed under the GNU General Public License (GPL), the commercialized Kasklimaat Model (KKM) model source code must be made freely available to customers and may be freely distributed thereafter [28].

### Mesh Generation

The mesh is modeled three-dimensionally to account for the three-dimensional behavior of turbulent flows. While many greenhouse climate models are developed in 2-dimensions, when wind is not perpendicular to the opening surface, 3-dimensional simulations more realistically represent the circulation patterns inside a greenhouse [12], such as the exchanges between staggered leeward and windward facing windows.

OpenFOAM's SnappyHexMesh utility was used to snap the environment grid around the imported greenhouse Stereolithography (STL) file developed in Sketchup. Meshes generated by the Snappy-HexMesh utility contain hexahedra and split-hexahedra derived from triangulated surface geometries. Simulating various window opening angles and wind approach angles was achieved in this work by generating a different mesh for each situation. The different window opening geometries and greenhouse orientations were modeled in Sketchup and meshed in the same computational domain.

The mesh grids were developed with finer cells near the greenhouse structure and along the ground (where strong gradients are expected to occur from cell to cell), while cells are coarser further away from the greenhouse, where relatively fewer changes in the flow are expected. This optimal mesh arrangement minimizes the necessary computational cost while maintaining solution accuracy. In order to minimize truncation errors, gradual variations in cell size were used within the grid. Cell volumes generally ranged between 5e-5 and 12.5  $m^3$ .

The following methods in OpenFOAM were used to develop the mesh in Figure ??b.

- External computational domain dimensions, grid density, and external patches (i.e. earth, atmosphere, inlet, outlet, and surrounding) were defined

- New mesh generated using the snappyHexMesh utility to snap the external environment grid to the greenhouse STL geometry modeled in SketchUp (Figure ??a).
- TopoSet utility used to select and group greenhouse faces (walls, ceiling and floor) within the mesh
- CreatePatch used to specify greenhouse boundary patches according to groupings from topoSet. These patches are later used to define boundary conditions when running simulations.

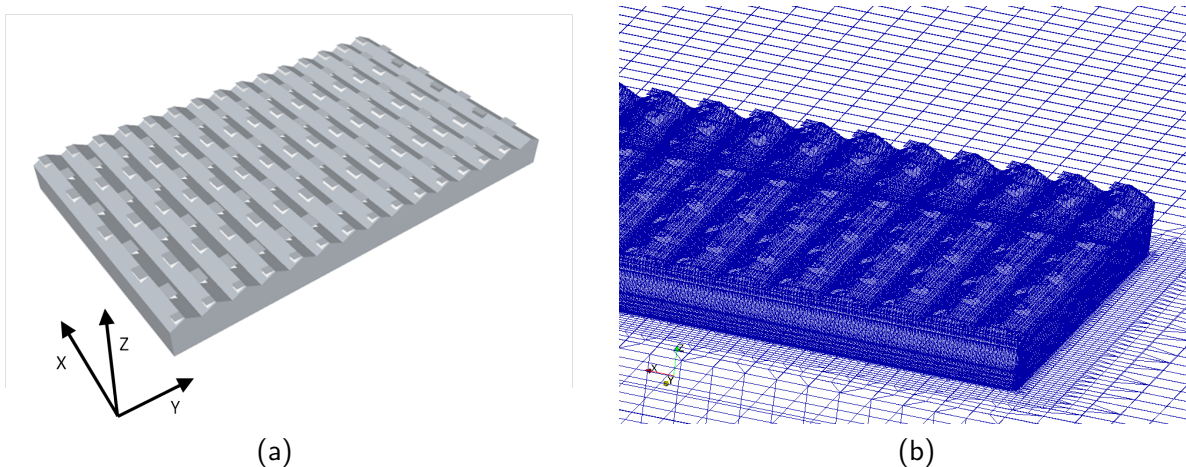


**Figure 4-1:** 3-Dimensional greenhouse model developed in SketchUp (a) and integrated into the mesh (b)

## Computational Domain

The boundaries of the mesh containing the environment surrounding the greenhouse can influence the simulation results. The computational domain must be large enough to encompass the largest relevant flow structures. Furthermore, if the cross-section is too small, artificial acceleration occurs around the object of interest. As a rule of thumb: the area of concern should be less than 10% of computational domain[29]. The selected blockage (ratio of projected greenhouse area in the flow direction to the computational domain cross section) is 5%. Following the recommendations of Blocken et al., the computational domain ratios are equivalent to the greenhouse cross-section [30]. The extension of the domain in the flow direction is 4 times the height of the greenhouse, as suggested by The Association of German Engineers (VDI) [29]. The outflow boundary should be far enough away from the object of interest that flow does not enter through this boundary, as this would hinder or even prevent convergence [31]. To allow the flow to redevelop after the greenhouse and prevent backflow, the outflow boundary is located at a distance of 15 times the height of the greenhouse. Figure 4-2 presents an over

## 4-1 Boundary Conditions

The constraints set for the various external environment calculations are inlet velocity profile, a prescribed pressure outlet, no-slip conditions along surfaces, and  $k$  and  $\epsilon$  wall functions. The non-uniform inlet wind profile is directed perpendicular to the flow. Details of the boundary conditions can be found in Table A-1 of the Appendix.

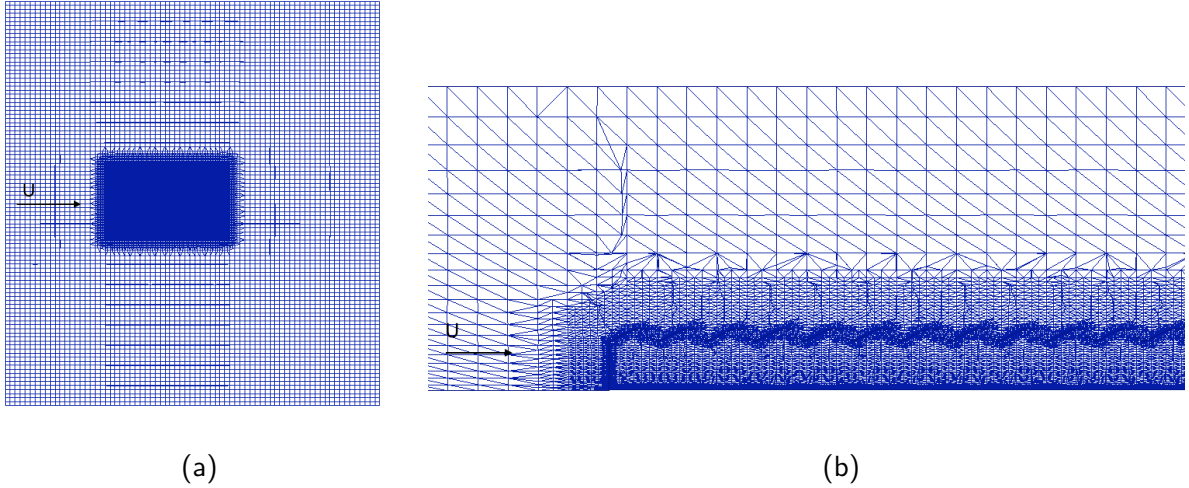


**Figure 4-2:** Overview of computational domain from the top and side views

### Fully developed Atmospheric Boundary Layer (ABL) profile resulting from the k-epsilon model

The wind velocity profile at the inlet of the model exhibits higher velocities farther away from the ground as a result of frictional drag. The widely adopted profile is based on Richards and Hoxey's work [32], which assumes the vertical velocity to be zero, the pressure to be constant in the vertical and streamwise directions, and the shear stress to be constant throughout the boundary layer. While wind is driven by large pressure differences, constant pressure can be assumed for the derivation of the atmospheric boundary layer profile because the pressure differences are very small over small segments of the vertical and horizontal dimensions:

$$U(z) = \frac{u_*}{K} \ln \left( \frac{z + z_0}{z_0} \right) \quad (4-1)$$

The turbulent kinetic energy  $k$  is defined by

$$k = \frac{u_*^2}{\sqrt{C_\mu}} \quad (4-2)$$

and turbulent kinetic energy dissipation is

$$\epsilon = \frac{u_*^3}{K(z + z_0)} \quad (4-3)$$

where the friction velocity  $u_*$  is calculated from a velocity  $U_h$  at a reference height  $h$ .

$$u_* = \frac{K U_h}{\ln(\frac{h+z_0}{z_0})} \quad (4-4)$$

$z$  is the vertical height,  $K$  is von Karman's constant (0.4), and  $z_0$  is surface roughness length. The input values for the atmospheric boundary layer profile are identified in Table 4-1.

## 4-2 Numerical Approach

The fvSchemes and fvSolutions files used by OpenFOAM to set numerical schemes and equation solvers can be found in Appendix B. The details of these two documents are discussed in the following two subsections.

**Table 4-1:** ABL Conditions

Variable	Variable	Value
Reference Velocity	Uref	5.5
Reference Height	Href	30
Surface Roughness Length	z0	uniform 0.1
Turbulent Kinetic Energy	turbulentKE	0.50497
Turbulent Kinetic Energy Dissipation	turbulentEpsilon	0.1734
z-axis Orientation	zDirection	(0 0 1)
Minimum coordinate value in z direction	zGround	uniform 0

### 4-2-1 Solution and Algorithm Control

The simpleFoam solver was initially used to simulate fluid flow in the external environment. This is a steady-state solver for incompressible, turbulent flow. However, it became apparent that the transient characteristics of the situation prevent the model from converging, and a transient solver can better achieve a solution. Therefore, the Pressure Implicit with Splitting of Operators (PISO) algorithm described in the theoretical background was used for the wind flow simulations presented. The pisoFoam solver models fluid characterized as incompressible, transient, and turbulent. Three pressure correction iterations and one non-orthogonal corrector were used during these calculations. The realizable  $k - \epsilon$  turbulence model (also presented in the theoretical background) was used for turbulence modeling.

#### Linear Solvers

The pisoFoam solver using the realizable  $k - \epsilon$  turbulence model solves equations for velocity, pressure, turbulent kinetic energy, and turbulent kinetic energy dissipation. Each discretization equation uses linear solvers to solve a set of linear equations (not to be confused with application solvers, which define the set of equations and algorithms). The Preconditioned Conjugate Gradient (PCG) linear solver is used to solve the symmetric pressure matrix equation using a Diagonal Incomplete-Cholesky (DIC) preconditioner. However, the Generalized Geometric-Algebraic Multi-Grid (GAMG) linear solver would have been more ideal. This method generates a fast solution for a selection of cells, which is then mapped onto a finer mesh as the initial guess for the solution. The velocity, turbulent kinetic energy, and turbulent kinetic energy dissipation all use the Gauss Seidel smooth solver. Smooth solvers reduce oscillatory error and transfer "smooth" error to coarse grids. While the Gauss Seidel method is one of the more reliable smooth solvers, it is relatively slow due to its sequential nature. A preconditioner, such as Preconditioned bi-Conjugate Gradient (PBiCG), could have considerably reduced the number of iterations for solving these sets of equations.

#### Convergence Criteria

With each iteration of the solvers, the residual error is evaluated. The solver stops when one of the following is satisfied.

- the residual falls below the solver tolerance,

- the ratio of current to initial residuals drops below the solver relative tolerance,
- or the number of iterations exceeds the specified maximum number of iterations.

The tolerances used are listed in Table 4-2.

**Table 4-2:** Residual error tolerances used in the PISO algorithm for each parameter

Parameter	Relative Tolerance	Absolute Tolerance
Velocity, $U$	0.1	1e-8
Pressure, $p$	0	1e-6
Turbulent kinetic energy, $k$	0.1	1e-8
Turbulent kinetic energy dissipation, $\epsilon$	0.1	1e-8

A pressure relative tolerance of zero indicates that the tolerance is calculated solely on the basis of the relative tolerance. A higher pressure tolerance was used in order to speed up the pressure correction steps.

## 4-2-2 Numerical Schemes

Table 4-3 provides details about the discretization schemes used for the calculation.

**Table 4-3:** Numerical Schemes

Calculation	Scheme
Time	Backward (second order, implicit)
Gradient	Gauss linear (second order, Gaussian)
Divergence	Gauss linear (second order)
Laplacian	Gauss linear limited corrected 0.333
Interpolation	Linear
Surface normal gradient	Explicit non-orthogonal correction

The backward second order time scheme is used to maintain an accurate transient calculation.

Gradient terms,  $\nabla$ , are discretized using the standard finite volume discretization of Gaussian integration, requiring interpolation of values from cell centers to face centers. In this case, linear interpolation, more commonly known as central differencing, is used.

The divergence scheme,  $\nabla \cdot$ , which determines the convection term of a fluid,  $\nabla \cdot (\rho u)$ , can only be discretized using the Gauss scheme, along with an interpolation scheme. Generally, simulations were initialized using upwind (first order) interpolation to calculate a more stable flow field before upgrading to the more accurate linear (second order) interpolation scheme. Furthermore, the positive turbulent kinetic energy and turbulent kinetic energy dissipation scalars are bounded. Limited linear differencing is used for the velocity vector to account for direction.

Laplacian schemes discretize the Laplacian term,  $\nabla \cdot (\nu \nabla u)$ . The interpolation scheme specified for the diffusion coefficient is Gauss linear. The surface normal gradient uses the coefficient 0.333, which corresponds to limited non-orthogonal correction.

Surface normal gradient scheme,  $\nabla u$ , specifies the gradient of two adjacent cell centers normal to the face between the two cells. This scheme uses explicit non-orthogonal correction.

### 4-3 Simulation Methods

With a total of 15 window opening angle combinations and 6 wind approach angles, 21 calculations of various external environment conditions were simulated. The calculations were initialized by mapping the flow patterns from a "constant" simulation used for testing spatial convergence and computational domain accuracy. The "constant" simulation contains a greenhouse with both leeward and windward windows open at a 30 degree angle from the roof, and an azimuth angle of 0 degrees (approaching the greenhouse perpendicular to the roof).

Methods used to maintain stability in the calculations (particularly the cases with varied wind azimuth angle) were

- mapping a flow field from another simulation as the initial condition,
- initializing the flow with a first order calculation (in space), before calculating the flow using a more accurate second order calculation scheme
- altering the numerical schemes (i.e. increasing the number of pressure correctors, increasing the number of non-orthogonal correctors, and using more effective preconditioners), and
- creating a new mesh with restricted skewness and finer refinement ratios.
- maintaining a Courant (dimensionless transport of each time step) number below 1.

The following section uses multiple methods to evaluate the convergence of the 21 cases. More details about Courant number are discussed in the section to follow.

---

# Chapter 5

---

## Verification and Validation of Results

This section presents observations which verify that the simulations accurately implement the conceptual theory modeled, and further validate the model's representation of physical reality.

### 5-1 Verification

Verification assessments are critical for determining correct implementation of conceptual models and whether the results can be used in an analysis of the boundary condition. The following methods are used to verify the simulations in this work [33]:

- Examine spatial (grid) convergence
- Examine temporal convergence
- Examine the implementation of the model
- Examine iterative convergence
- Examine consistency

#### 5-1-1 Examine Spatial Convergence

Two tests were done to ensure mesh accuracy. Resolution independence was tested by running the solver with the same boundary conditions in a coarser and finer mesh, containing twice as many cells in each dimension. Similarly, the effect of the computational domain was tested by increasing the dimensions in each direction by a factor of 2.

#### Computational Domain

To ensure that the computational domain is large enough to avoid artificial acceleration, tests were conducted to optimize mesh accuracy. Figures 5-1 and 5-2 depict the top and side views of the larger computational domain examined.

Two points were selected to investigate error between the two calculations. At a point located at the center of a windward facing window, the velocity magnitude of the smaller computational domain

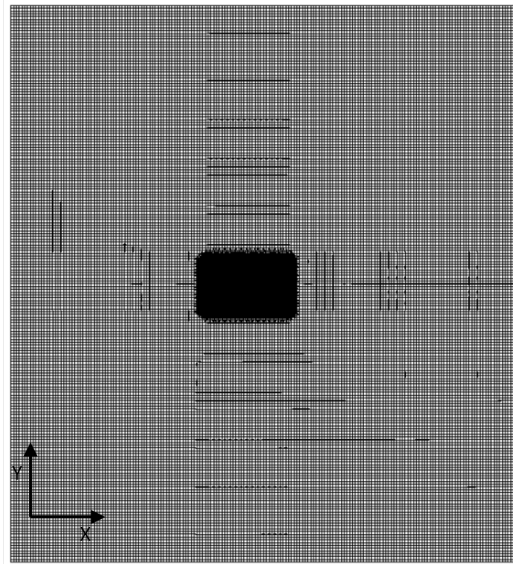


**Figure 5-1:** Top view of larger computational domain, twice as long in each dimension (370m x 400m)

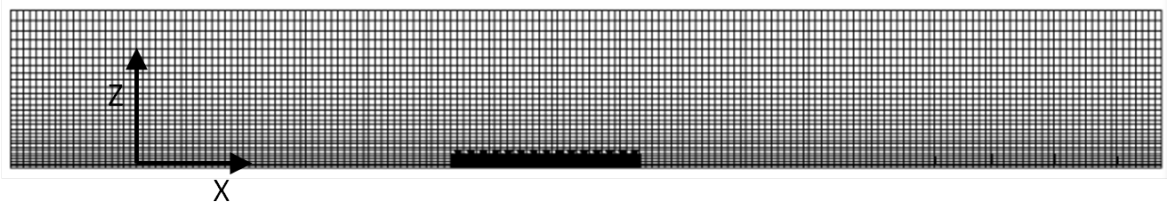


**Figure 5-2:** Larger Computational Domain Mesh, twice as long in each dimension (370m x 50m)

is 38.8% below the velocity of the larger computational domain. However, at a point located along the floor of the greenhouse, the velocity calculated in the smaller computational domain is 62.1% above the velocity calculated for the larger computational domain. The zoomed in velocity profiles for a slice in both the large and small computational domains can be seen in Figures 5-3 and 5-4, respectively.

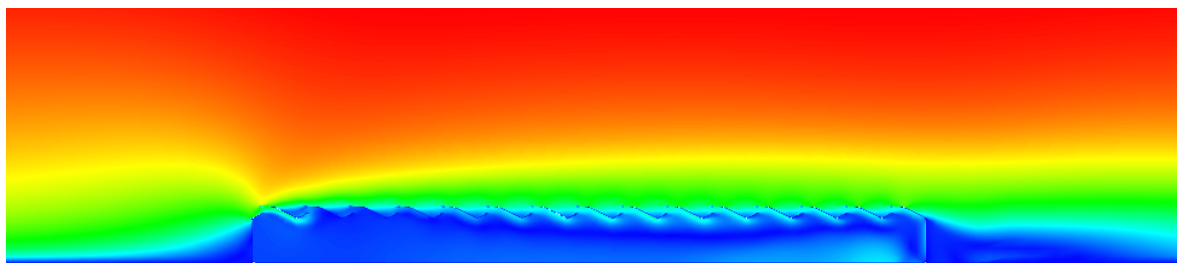


**Figure 5-3:** Velocity magnitude flow field in the larger computational domain

The two flow fields are presented with matching scales. It is apparent that the larger computational domain models lower velocities within the greenhouse. Furthermore, there appears to be some artificial acceleration present in the smaller computational domain. When animated over time, the flow within the greenhouse is not steady. Therefore, the smaller computational domain was used for the parametric tests ventilation tests due to time limitations. Qualitatively, the various greenhouse simulations can be expected to show reasonable flow trends, with low velocities near the windward side of the greenhouse and higher velocities at the floor near the leeward side of the greenhouse. However, given the transient nature of the flow, the results will most accurately represent mean flow

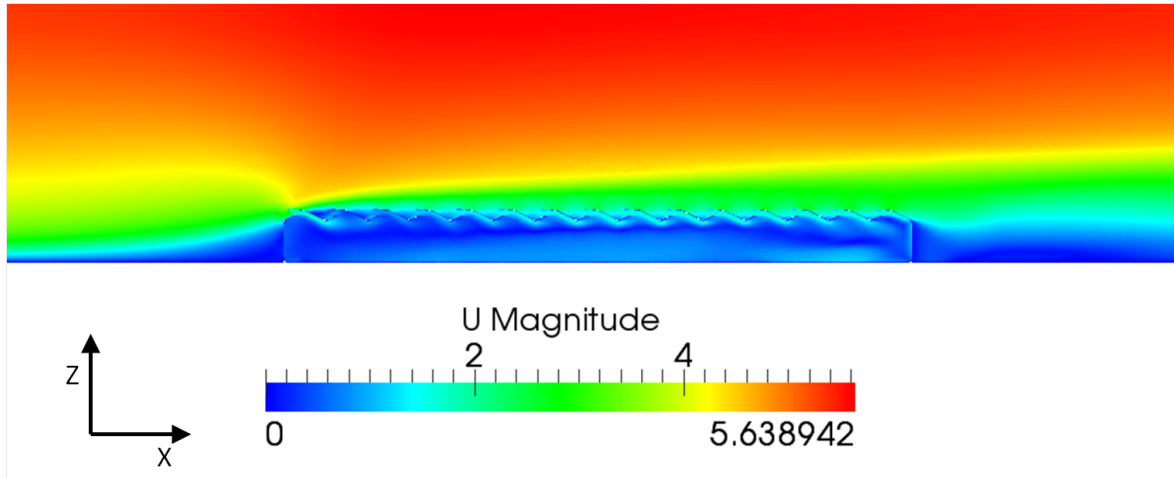


**Figure 5-4:** Velocity magnitude flow field in the computational domain

fields, rather than flow fields at a given time.

### Mesh Fineness and Spatial Convergence

The performance of high Reynolds turbulent flow calculations is dependent on cell size near the wall, in order to accurately represent the approximate logarithmic behavior of velocity near walls due to friction. However, wall functions can also be used to account for this behavior using experimental correlations based on wall roughness. Wall functions, however, remain a boundary condition in this work to optimize the model accuracy (particularly of turbulence quantities), a common practice among greenhouse climate studies [12].

To ensure that the mesh cells are fine enough to minimize discretization error, tests were conducted to optimize the mesh accuracy (within the computational limits of TNO's computing equipment). A flow field was computed for three grids, each with twice the number of grid points in each dimension of the previous grid. With each level of grid refinement, the spatial discretization errors should asymptotically approach zero.

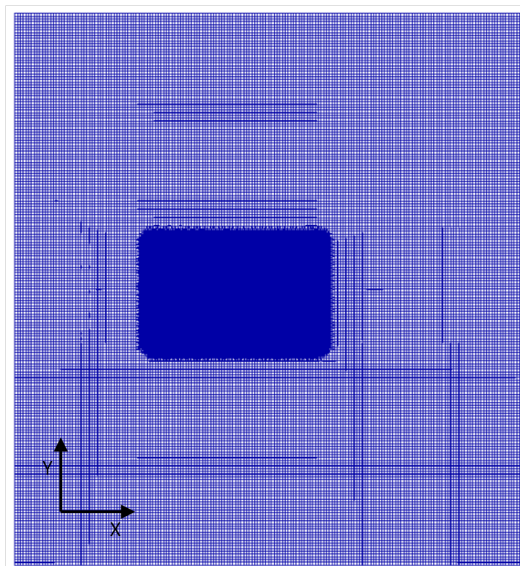


**Figure 5-5:** Top view of finely meshed grid with twice as many cells in each dimension (185m x 200m)

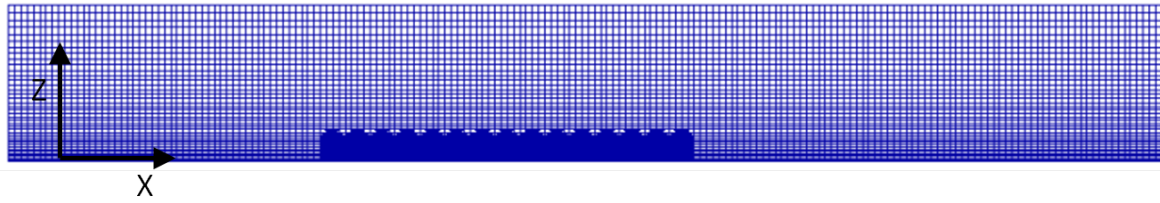


**Figure 5-6:** Side view of finely meshed grid with twice as many cells in each dimension (185m x 25m)

Table 5-1 below indicates the grid details and the resulting pressure coefficient computed at a single point located in the opening of a windward facing window in the center of the first span of the greenhouse.

**Table 5-1:** Spatial convergence details

Normalized Grid Spacing	Pressure Coefficient, $C_p$
1	0.2694
2	0.2515
4	-0.0201

From these values, the observed order of convergence is determined. The error can then be defined as the difference between the discrete and exact solutions.

$$E = f(h) - f_{exact} = Ch^p + \text{HigherOrderTerms} \quad (5-1)$$

where  $f$  is a calculated quantity (velocity, pressure, etc.),  $C$  is a constant,  $h$  is a grid spacing measure, and  $p$  is the order of convergence. For a second order discretization scheme, the order of convergence,  $p$ , would be 2. In this case, the numerical CFD schemes provide a theoretical second order of convergence. However, an observed order of convergence,  $p$ , is usually lower as a result of boundary conditions, numerical models, and the grid. Neglecting higher order terms, Equation 5-1 can be rewritten as

$$\log(E) = \log(C) + p \log(h) \quad (5-2)$$

by taking the logarithm on both sides of the equation. The format of this equation indicates that the order of convergence is the slope of the curve of  $\log(E)$  and  $\log(C)$ . While a least squares fit could be used to determine this value, a more accurate method for such few data points would be to assume a constant grid refinement ratio,  $r$  with Equation 5-3.

$$p = \frac{\ln \frac{f_3-f_2}{f_2-f_1}}{\ln r} \quad (5-3)$$

where  $r$  is the grid refinement ratio,  $r = h_1/h_2$ . The pressure coefficients provided in Table 5-1 result in an order of convergence of 3.92, while the expected order is 2. This indicates that the three calculations are not in the asymptotic range of convergence.

Richardson extrapolation, a method based on Taylor series representation, uses the observed order of convergence,  $p$ , to estimate a value at zero grid spacing using lower-order discrete values [33]. The continuum value can be obtained by

$$f_{h=0} \cong f_2 + \frac{(f_1 - f_2)r^p}{r^p - 1} \quad (5-4)$$

For the quantities given in Table 5-1, the Richardson extrapolation method estimates a zero grid spacing pressure coefficient of 0.2707. However, given that the three calculations are not in the asymptotic range of convergence, a more reasonable order of convergence of 1.7 (rather than 3.92), would result in a zero grid spacing pressure coefficient of 0.2774. The values are plotted in Figure 5-7

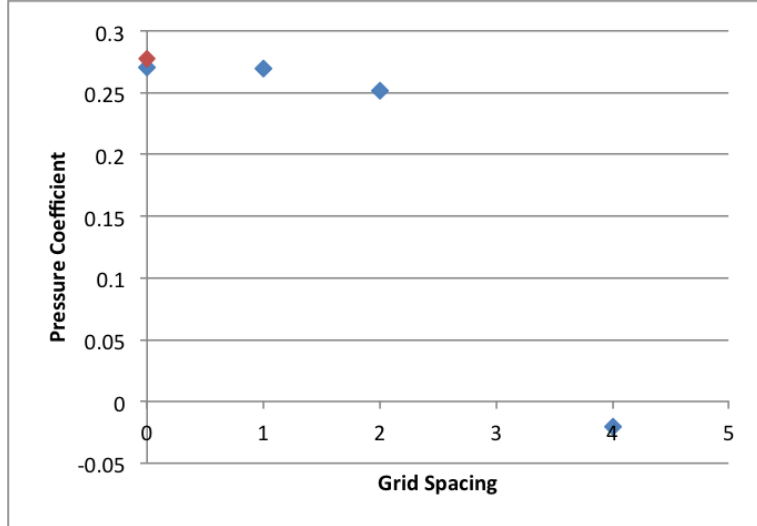


**Figure 5-7:** Spatial convergence study. The value in red indicates the Richardson extrapolation for an assumed order of convergence of 1.7

The method can also be used to estimate the discretization error of values obtained from CFD. The estimated fractional error of the fine mesh is defined as

$$E_1 = \frac{\epsilon}{r^p - 1} \quad (5-5)$$

where the relative error is given as

$$\epsilon = \frac{f_2 - f_1}{f_1} \quad (5-6)$$

intermediate mesh is defined as

$$E_2 = \frac{\epsilon * r^p}{r^p - 1} \quad (5-7)$$

Based on values reported in Table 5-1, the estimated fractional error for calculations using the fine mesh was determined to be 0.0047, while the fractional error for the intermediate grid refinement is 0.071. Assuming an order of convergence of 1.7 (rather than 3.92), the error becomes 0.030 and 0.096 for the fine and intermediate grids, respectively. Despite the increased error, for the purpose of this work, the intermediate mesh refinement will be used, given the available computational power and limited time.

### 5-1-2 Examining Temporal Convergence

Temporal accuracy and numerical stability of transient flows are dependent on mesh fineness. The Courant number,  $Co$ , represents the dimensionless transport for each time step, and must be kept below 1.

$$Co = \frac{U\Delta t}{\Delta x} \quad (5-8)$$

Monitoring the Courant number (discussed in Section ??) and maintaining a value below 1 was the main method used to stabilize the calculations and monitor convergence. To achieve this, time steps ranged from 0.001 to 0.01 seconds. The Courant value was constant throughout the calculation with negligible fluctuations when window opening angle was varied. In some cases, a very low time step was necessary for the first few time iterations. The time step was later increased as the solution stabilized, in order to speed up the calculation. Sudden jumps were observed in the Courant value throughout the calculations for various wind azimuth angle, although the maximum value remained below 1 for nearly all iterations. These calculations often required smaller time steps to maintain a Courant value close to 0.5, avoiding spikes in excess of 1. These spikes are likely caused by errors within the mesh, such as skewed cells and adjacent cells of difference fineness ratios. An example of the monitored Courant value for an azimuth angle of 75 degrees, compared with a 0 degree azimuth angle can be found in Figure 5-8.

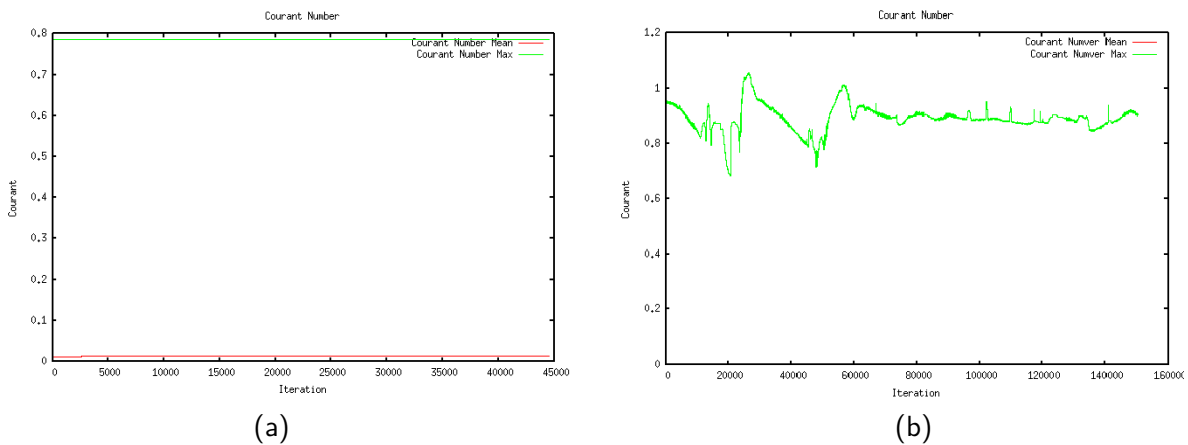


**Figure 5-8:** Monitoring Courant value for (a) 0 and (b) 75 degree wind azimuth angles at each time step. This image shows the degree of Courant fluctuations when calculating varied wind approach angles, in comparison to the constant Courant number throughout calculations of varied window opening angles.

### 5-1-3 Examine the Implementation of the Model

This verification method requires an investigation of the simulation calculation visually and experimentally. This evaluation revealed that one of the simulations was redundant. The simulation containing closed windward-facing windows and 15 degree leeward-facing windows contained an error in the greenhouse geometry, modeling instead 15 degree windward facing windows and closed leeward facing windows. Therefore, the effect of closed windward-facing windows and 15 degree leeward-facing windows cannot be included in the analysis.

### 5-1-4 Examine Iterative Convergence

Given the iterative nature of Computational Fluid Dynamics (CFD) calculations using the Pressure Implicit with Splitting of Operators (PISO) algorithm, monitoring the convergence is necessary in order to obtain an accurate solution. Within the PISO algorithm, residual error tolerances were set either as absolute or relative tolerance for each model parameter (Table 4-2).

#### Time Step Residuals

An example of the monitored initial residual for the calculated parameters and continuity is presented in Figure 5-9.

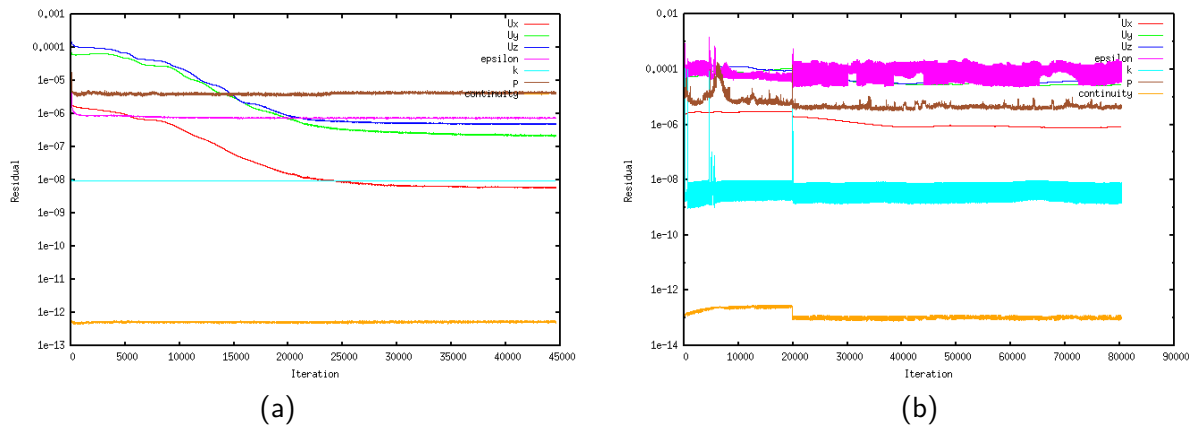


**Figure 5-9:** Initial residual error for each time step for (a) a zero degree wind approach angle and (b) a 75 degree wind approach angle

The time step was increased for several cases following initial stabilization, to speed up the calculation. Increasing the time step resulted in an initial increase in the residual error, followed by a steady decrease. In other situations, it was necessary to decrease the time step, in order to lower the Courant number and the residual error (as seen in Figure 5-9b). While residual error decreased below 1e-5 for the cases where window opening angle was varied, the wind azimuth angle cases produced larger residual error (sometimes exceeding 1e-4). This residual could have been reduced by lowering the time step, however, time constraints prevented the time step from being further decreased. The residual error could also have been altered by using a different initialization field. The higher residual error for the wind azimuth angle cases indicates that convergence has not been reached, and close attention should be paid in the verification and validation of these calculations.

#### Integral Values

Stationarity of external flow is determined both visually and theoretically. Animating time steps of planes parallel to the wind direction can be valuable for observing flow stabilize and vortex shedding. Further observations of convergence can be deduced by evaluating integral quantities over the greenhouse (lift, drag, and yield). Sometimes, it is possible that these external forces converge before residual decreases and stabilizes. Therefore, this test is can be useful for evaluating the convergence of the azimuth angle calculations.

The temporal fluctuations and stabilizing of the drag coefficient are depicted in Figure 5-10. The drag coefficient is a ratio of the drag force to the product of dynamic pressure and area.

$$C_d = \frac{F_d}{\frac{1}{2}\rho U^2 A_{ref}} \quad (5-9)$$

where  $F_d$  is the drag force,  $\rho$  is density,  $U$  is the velocity far away from the greenhouse at the height of the window, and  $A_{ref}$  is the reference cross sectional area, taken as the projected greenhouse on a plane whose normal points in the direction of the wind. Drag force,  $F_d$ , is the sum of the viscous drag and pressure drag forces ( $F_d = F_v + F_p$ ). These two forces are integral quantities calculated in OpenFOAM over the entire greenhouse surface. The viscous force is proportional to the air speed,  $u$ , greenhouse surface area,  $A$ , and inversely proportional to separation,  $z$ :

$$F_v = \mu A \frac{u}{z} \quad (5-10)$$

where  $\mu$  represents dynamic viscosity. The pressure force is given as

$$F_p = pA \quad (5-11)$$

where  $p$  represents the pressure on a surface with area,  $A$ .

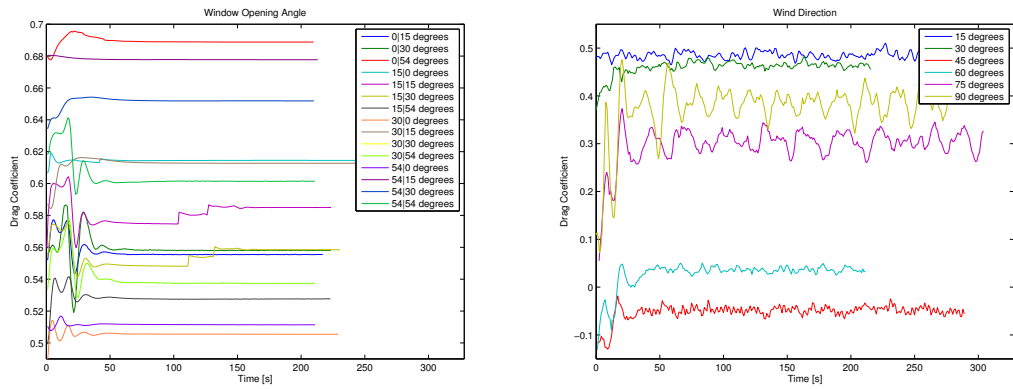


**Figure 5-10:** Temporal fluctuations of drag coefficient for variations in window opening angle (left) and variations in wind direction (right)

The highest drag forces occur when either a windward or leeward facing window is completely open (54 degrees). When compared with the varied window opening simulations, the varied wind direction simulations have a very unsteady drag coefficient, although the drag fluctuates over a constant mean value. Figure 5-11 breaks down the drag coefficient into pressure and viscous components. While pressure drag coefficients appear stable, (despite fluctuations for window directions), the viscous coefficients are not completely stable for wind azimuth angle simulations. However, it is important to recognize that the viscous forces have a much smaller magnitude, and therefore have little influence on drag force. There is an unexpected negative pressure drag coefficient for the 45 degree wind approach angle calculation, which results in a negative drag coefficient. This indicates that the calculation has likely not yet reached convergence, an argument that is further supported in the following sections.

### Flow Parameters Near Windows

Given that the focus of this work is to evaluate the flow fields near the windows of the greenhouse, it is necessary to perform a more detailed analysis of stationarity at the window openings. While monitoring the residual for each time step can be valuable, it is also important to monitor the

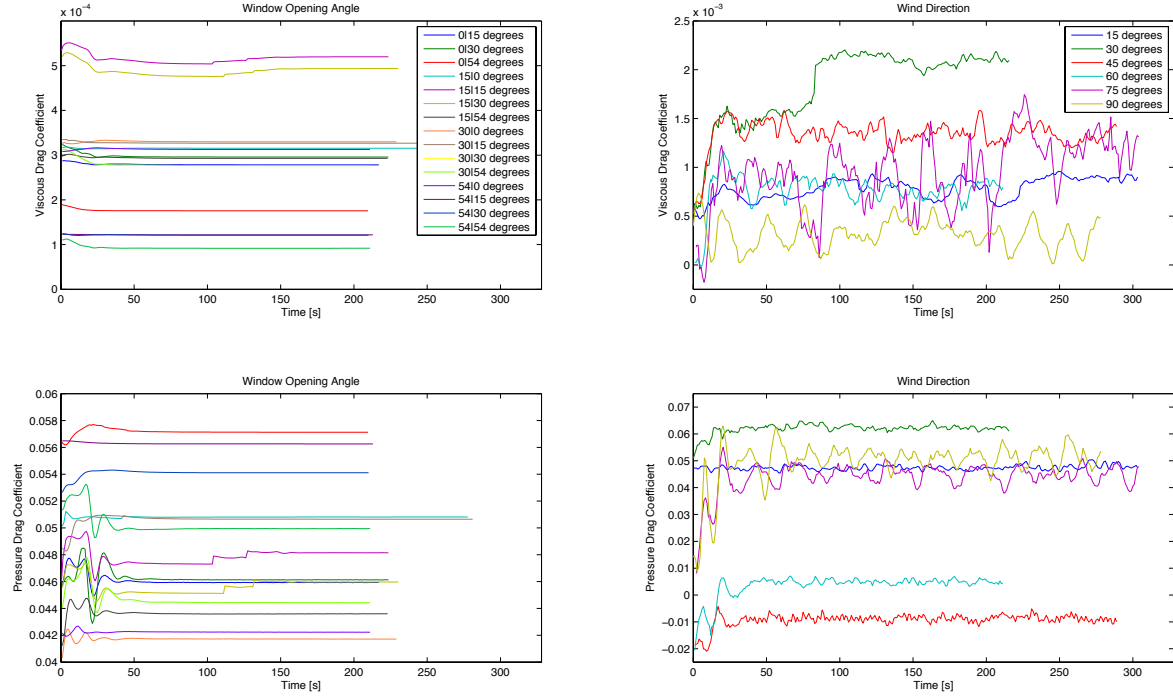


**Figure 5-11:** Temporal fluctuations of drag coefficient for variations in window opening angle (left) and variations in wind direction (right), broken down by pressure and viscous forces

parameter values over time to ensure that a sufficient number of time steps have allowed the calculation to overcome the high variance due to unphysical initial conditions. Figures 5-12 and 5-13 give an example of several values measured over time probed at various window openings of the "constant" run and a 75 degree wind azimuth angle respectively. From the constant run, it is evident that fluctuations due to initialization take place during the first 80 seconds. However, there remain some minor fluctuations throughout the remaining duration of the calculation due to the transient nature of the flow. A similar trend was observed for the simulations of varying window opening angles.

Alternatively, there is higher variance in the varied wind azimuth angle calculations. The reduced time step in the first 50 seconds (consistent with the residuals plot in Figure 5-9b) indicates slightly more stable calculations, although large fluctuations are still abundant. The large jumps in turbulence quantities (at time = 40 seconds, for example) are an indication that smaller flow features are resolved due to a reduction in the time step. When the time step is reduced, the small scale turbulent motion with fast time scales can be resolved. A time scale for the small eddies,  $t_{eta}$  can be estimated with

$$t_\eta = \left( \frac{\nu l}{u^3} \right)^{\frac{1}{2}} \quad (5-12)$$

with velocity,  $u$ , length scale,  $l$ , and kinematic viscosity,  $\nu$ . Therefore, halving the time step, would reduce the length scale of resolved turbulence features by one quarter (provided they can be spatially resolved with a Courant number below 1). The change in turbulence kinetic energy and turbulent kinetic energy dissipation values in Figure 5-13 is in accordance with the change in length scale. Resolving  $k$  and  $\epsilon$  for different sized flow features results in a significant change for some values but smaller change for others, because the size of turbulent eddies varies throughout the flow region. Similar observations were made for the five other varied wind approach angle simulations.

In both Figures 5-12 and 5-13, the turbulent kinetic energy,  $k$ , is constant, while the expected

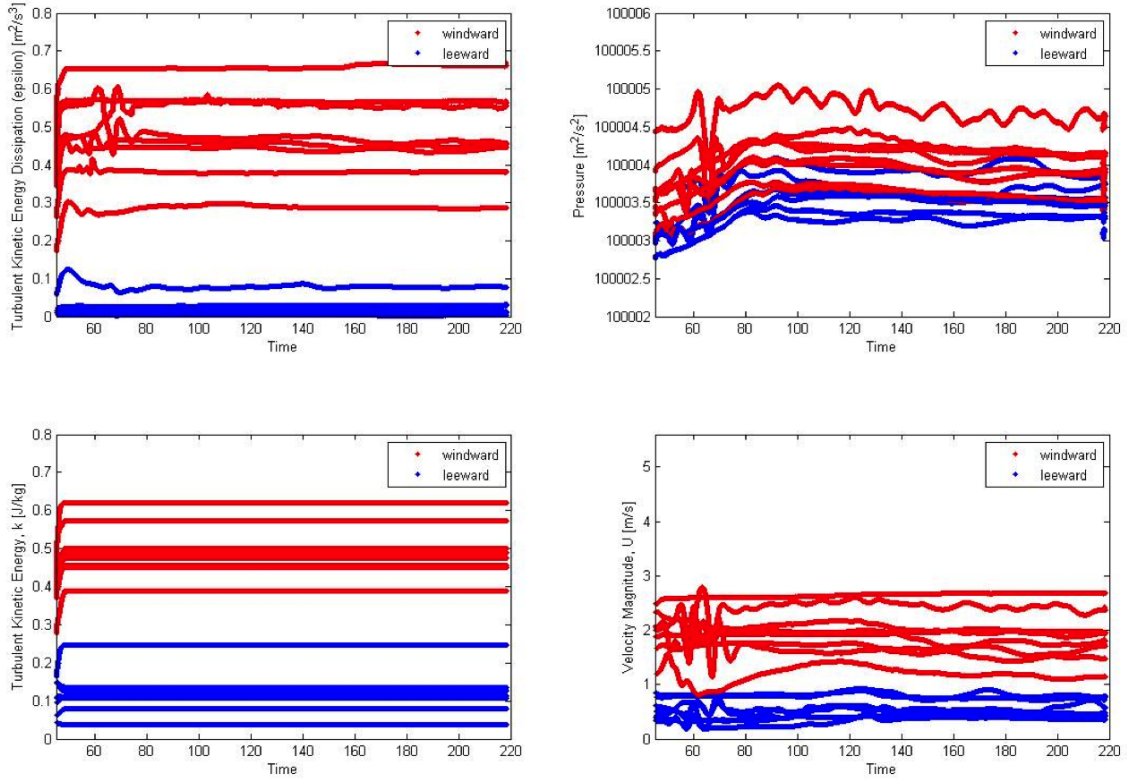


**Figure 5-12:** Temporal fluctuations of calculated fields colored by window direction for a 0 degree wind approach angle and 30 degree window openings

behavior would follow the fluctuations of the velocity, given the dependence of turbulent kinetic energy on velocity in Equation 2-20. This error is due to the high tolerance set in Table 4-2 for turbulent kinetic energy. As a result, the solver does not solve for this field at each time step. This is further confirmed by the residual plot in Figure 5-9, which shows an initial turbulent kinetic energy residual below 1e-8 for each time step. A lower tolerance for  $k$  would have produced more physical results, but would have also increased the computation time.

Further investigation into the stationarity of the calculations over the latest 30 seconds of computation time can be determined with regression modeling. To test that the simulations are statistically stationary, a regression model

$$U_{mag} = C + \beta t, \quad (5-13)$$

was fit to the velocity time series for all points sampled at the greenhouse windows (8495 probes for varied wind azimuth angle and 8665 for varied window opening angles).  $C$  represents the stationary velocity magnitude in  $\frac{m}{s}$ , with a rate of change,  $\beta$ , over time,  $t$ . A stationary velocity probe would have  $\beta = 0$ , indicating that fluctuations occur over a constant trend (rather than an increasing or decreasing trend).

The significance of the coefficient  $\beta$  was evaluated based on the p-value and the estimated  $\beta$  coefficient value. The p-value significance was judged according to the F-statistic of the hypothesis test that the corresponding coefficient is equal to zero. A p-value below 0.05 rejects this hypothesis.  $\beta$  coefficients within the range of  $\pm 0.0033 \frac{m}{s^2}$  (indicating a an increase or decrease in velocity by 0.1 m/s over a 30 second period) were also considered insignificant. The resulting percentage of stationary window probes are listed in Tables 5-2 and 5-3.

Nearly all probed points in the the window opening angle calculations were found to be stationary according to the specified criteria. However, the wind azimuth angle calculations are not stationary. This is due to the initialized flow fields. It appears that the degree to which the initialized greenhouse

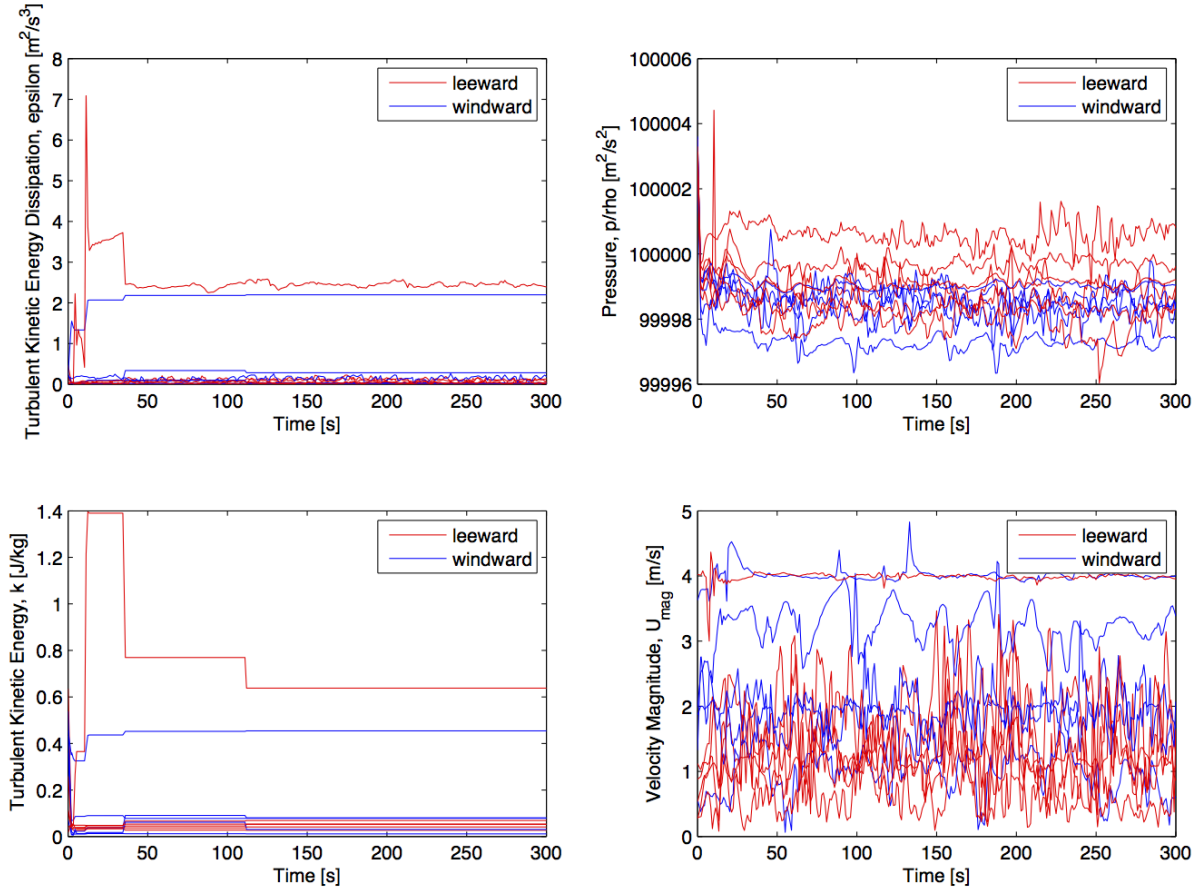


**Figure 5-13:** Temporal fluctuations of calculated fields colored by window direction for a 75 degree wind approach angle and 30 degree window openings

structure overlapped with the rotated greenhouse influences the number of stationary probes. A 15 degree azimuth angle has the largest amount of overlap with the 0 degree azimuth angle initialization field, and therefore has the fewest stationary calculations at the windows. Alternatively, the 75 and 90 degree wind azimuth angle calculations have the highest percentage of stationary probes, due to the smaller overlap of the rotated and 'mapped' greenhouses.

The analysis of CFD calculations in this work is based on the mean values and their standard deviations over the latest 30 seconds worth of time steps (found in Appendix ??).

### 5-1-5 Examine Consistency

Verification of simulation consistency involves an investigation of whether the simulation initial conditions change over time and an evaluation of the net flux through the windows.

#### Comparison with Initial Conditions

In addition to low residual tolerances, inaccurate initial conditions require the calculation to run for a sufficient number of time steps before reasonable results are produced. Calculations for all 21 variable cases (varying window angles and wind directions) of the external environment were run for a minimum of 3.5 minutes of computational time, allowing enough time for the calculated fields to stabilize and for initial residual error to be sufficiently low.

**Table 5-2:** Percentage of stationary window probes in varied wind azimuth angle calculations (with fixed 30 degree windward and leeward window opening angles)

Azimuth Angle	Stationarity
15	55.6%
30	57.1%
45	63.5%
60	64.5%
75	72.5%
90	72.2%

**Table 5-3:** Percentage of stationary window probes in simulations of varied window opening angle combinations (with fixed 0 degree wind approach angle)

		Leeward Angle			
		0	15	30	54
Windward Angle	0	100%	100%	100%	100%
	15	100%	100%	100%	100%
	30	100%	100%	99.4%	100%
	45	100%	100%	100%	100%
	54	100%	100%	100%	100%

In order to stabilize the varied wind azimuth angle simulations and minimize calculation time, the flow field of these calculations were initialized with the results from the 'constant' run, in which windows are open at 30 degree angles and wind approaches at a zero degree azimuth angle. In this section, the influence of the initial conditions is evaluated. Given that a ventilation boundary condition will be developed based on the flow at the windows, Figures 5-14 and 5-15 compare the initial and final velocity and pressure values at the windows of the greenhouse after 5 minutes of computation time.

There is a clear indication that after 5 minutes, the flow field still resembles the initial flow field (with the greenhouse rotated 75 degrees counterclockwise of the simulated greenhouse). This could be due to a longer time scale for internal flow compared to the external environment, requiring more time for the internal flow to converge. This hypothesis is further validated with Equation 5-12, in which the relationship between time scale and velocity ( $t_\eta \propto u^{-\frac{3}{2}}$ ) indicates lower velocities within the greenhouse are expected to have longer time scales compared to the higher velocities in the external environment. The low velocities near the greenhouse, coupled with the unsteadiness in the flow field, indicates that the solution time could take significantly longer to produce a flow field at the windows representative of a 75 degree wind azimuth angle. Furthermore, it is possible that the solver is simply unable to achieve a proper solution when starting from the applied initialization field.

The results of the azimuth angle calculations are deemed insignificant based on the high residual error, insufficient runtime (and remaining influence of initialization), and evidence that the turbulent kinetic energy is not solved correctly (due to a high residual tolerance setting). However, alternative

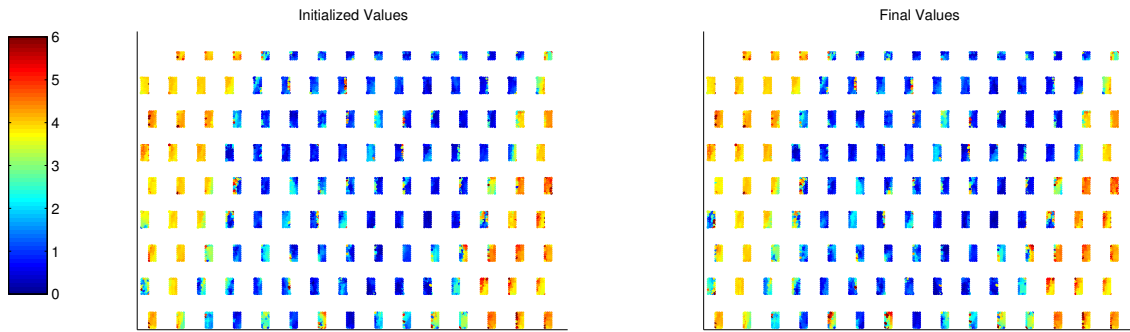


**Figure 5-14:** Comparison between initial and final velocity magnitude [m/s] at the window openings for the 75 degree wind azimuth angle simulation. The "final value" indicates a sample taken after 5 minutes of calculation.

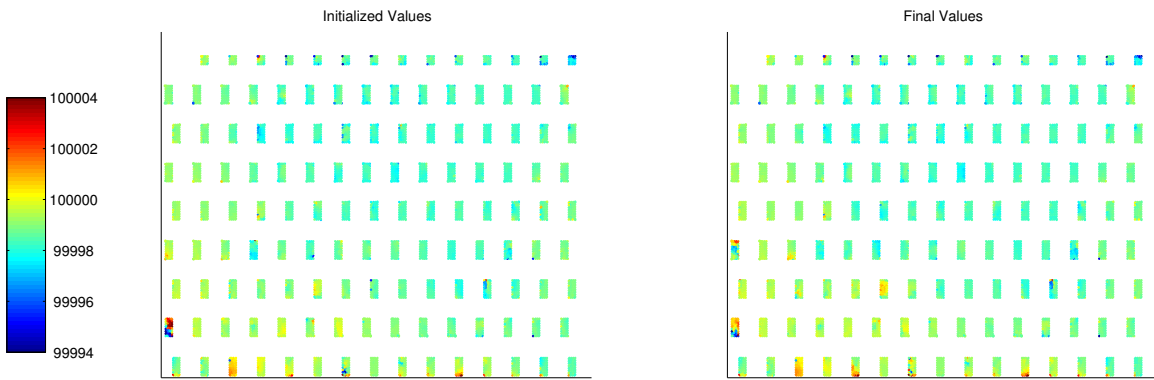


**Figure 5-15:** Comparison between initial and final pressure [ $\frac{m^2}{s^2}$ ] at the window openings for the 75 degree azimuth angle simulation. The "final value" indicates a sample taken after 5 minutes of calculation.

initialization methods, such as a calculation from a coarser grid, or the use of the PotentialFoam solver may have been better methods for initialization for the purpose of this study. These calculations can also be run for a longer duration to determine a more realistic flow pattern along the greenhouse roof once the calculation finally converges.

## Window Fluxes

A closer look at the flux through the windows can provide further detail about the greenhouse ventilation. The volumetric flow rate is determined using a mean velocity for each window.

$$Q = \vec{u}_{mean} \cdot d\vec{A} \quad (5-14)$$

where vector area,  $\vec{A}$  is a vector normal to the window surface, whose magnitude amounts to the window area,  $\vec{A} = A\hat{n}$ .

Figure 5-16 visualizes the fluxes at each window for all 14 calculations (recalling that an error in the greenhouse geometry required discarding the 15 degree leeward and closed windward facing window calculation). There are some unexpected trends observed for various window angles. Most

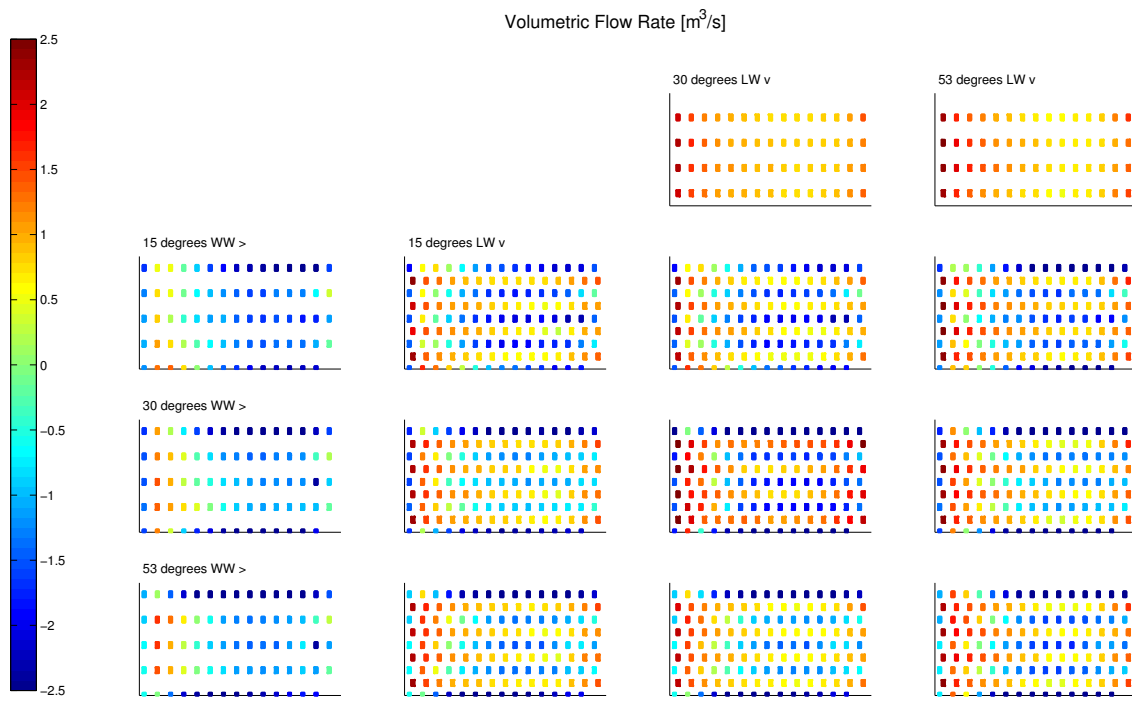


**Figure 5-16:** Volumetric flow rate at the plane of the windows for the 14 varied window opening angle simulations in  $m^3/s$ . The location of the greenhouse profile (row and column) determine the combination of windward (WW) and leeward (LW) opening angles, respectively. The first row represents simulations where the windward-facing windows are closed, while the first column represents leeward-facing windows that are closed. Due to errors in simulated greenhouse geometry, 15 degree leeward and close windward window opening angle simulation is not shown.

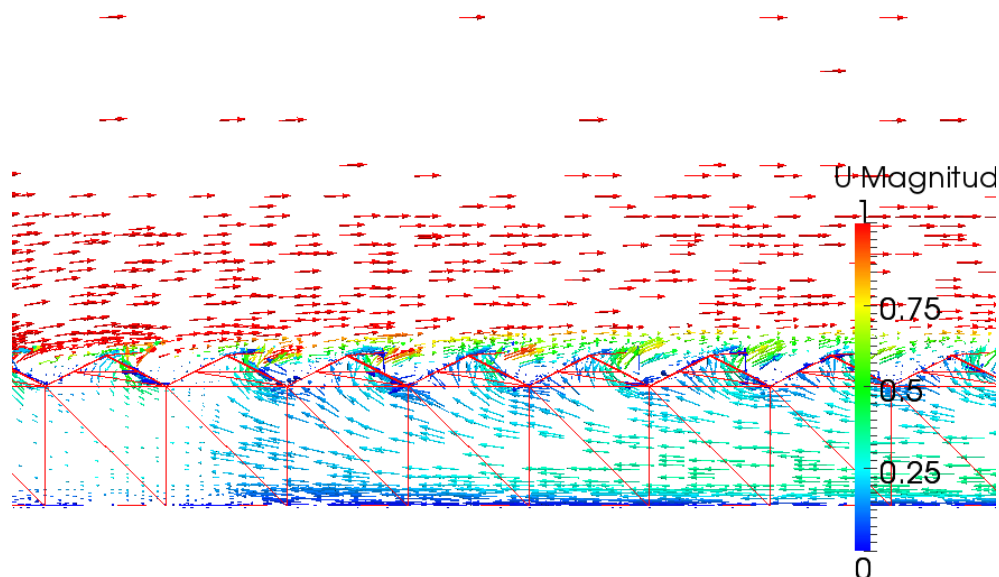


**Figure 5-17:** Vector plot of velocity for a slice located along the leeward facing windows in a simulation containing closed windward facing windows

obvious is in the first row and first column of greenhouse simulations, representing closed leeward,

and windward-facing windows, respectively.

When the windward-facing windows are closed, there is no inflow into the greenhouse. These results show that the continuity equation is not satisfied. A closer look at the vector plot for a slice along the leeward facing window in a simulation where the windward facing windows are closed (Figure 5-17) further validates this observation that purely outflow occurs in leeward facing windows.

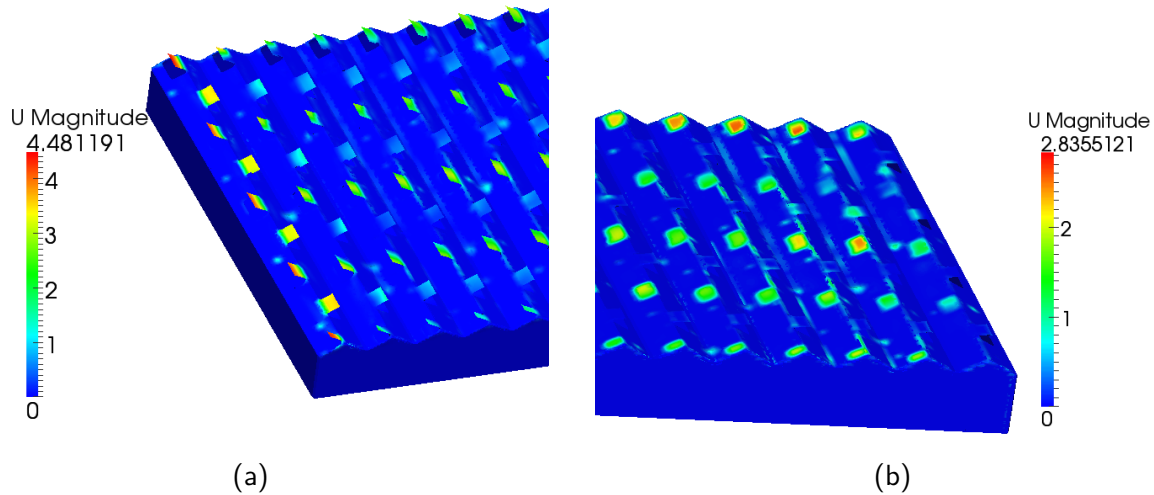


**Figure 5-18: f**

or the greenhouse geometry of (a) a simulation with 53 degree windward and leeward facing windows and (b) a simulation with closed windward and 30 degree leeward facing windows]Velocity boundary condition for the greenhouse geometry of

- (a) a simulation with 53 degree windward and leeward facing windows and (b) a simulation with closed windward and 30 degree leeward facing windows

This is caused by erroneous initialization of the flow field. Rather than just initializing the flow field for each window configuration, it is evident that the boundary condition of the greenhouse is changed from no slip conditions to the velocity of the initialized field. Therefore, a closed window acts as an imposed velocity directed into the greenhouse. A window open 100% imposes a velocity on the external flow of the greenhouse, rather than acting as a barrier to flow. The velocity boundary condition of the greenhouse structure for these two situations are presented in Figure 5-18. The imposed velocity where a closed window is expected results in outflow through the window openings in order to satisfy continuity.

The 'constant' case is still expected to have a mean flow rate of zero, given that no initialization error occurs at the greenhouse geometry for this case. However, when the volumetric flow rate at each window is summed, the result is a  $14.2 \text{ m}^3/\text{s}$  net inflow. This could be due to sampling limitations. The values sampled at the greenhouse windows are not evenly distributed over the window, while the volumetric flow rate in each is determined using an average velocity of the sampled values in each window. No leaks were found in the greenhouse geometry (aside from intentional window openings), and the boundary condition of the greenhouse was set to no slip conditions.

The inability to verify mass conservation consistency indicates that none of the data from the variable cases can be evaluated further due to erroneous initialization. Following the examination of spacial convergence, temporal convergence, model implementation, iterative convergence, and consistency, the only data that can be verified is the 'constant' case.

## 5-2 Validation

While verification showed that the constant simulation has converged, numerically, validation is necessary in order to show that the results are physically realistic.

Several experimental greenhouse ventilation studies have found consistent results with respect to inflow and outflow windows. They have found that airflow generally enters through downwind ventilators and exits through upwind ventilators, irrespective of wind speed and window opening angle [35] [36]. This pattern is observed in the results presented in the previous section.

Quantitative validations must compare the results to wind tunnel tests, or field tests where the velocity is large enough ( $> 2m/s$ ) that the buoyancy effect is negligible. While experimental field tests lack control over the external wind conditions (i.e. constant wind direction and wind velocity) to match with the present study, wind tunnel tests provide more control in this regard.

Given that the wind-induced pressure distribution over the greenhouse roof is the driving force for ventilation (neglecting buoyancy), Mistriotis et al. suggest that correct pressure differences predicted by CFD are an indication that ventilation pressures are accurately modeled [37]. This is a common practice within the greenhouse climate modeling sector, and is used to validate the ventilation models used to develop a ventilation boundary condition. Experimental measurements were collected by Wells and Hoxey [38] for a Venlo greenhouse with the same roof pitch as the greenhouse used for the calculations of this study. The experimental measurements correct for fluctuations in wind direction by assuming a quadratic relationship between pressure coefficient and wind direction. The weighted function was derived by minimizing residuals between wind load and  $(C_p \Delta q)$ . Figure 5-19(a) presents a comparison of the pressure coefficients for a closed roof calculation of the geometry used in this study.

While this validation method shows good agreement, the previous discussion of CFD turbulence calculation methodologies (RANS versus LES) indicates that the actual velocities calculated can still be inaccurate.

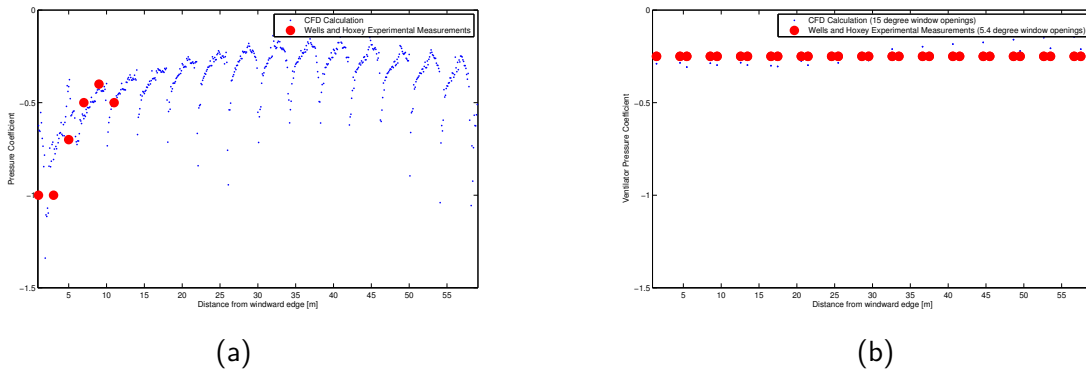


**Figure 5-19:** Pressure coefficient validation comparing the pressure distribution over a closed greenhouse roof (a) and over the window openings along a greenhouse roof (b)[38]

Wells and Hoxey [38] also determined a constant pressure coefficient for open windows (at a 5.4 degree opening angle). Despite a 24.6 degree difference in window opening angle from the measured data, Figure 5-19(b) compares the pressure coefficient to the CFD calculation. The values are plotted to the same scale as (a) to show that the pressure varies much less over window ventilators. When compared to the mean value for this window configuration determined by Wells and Hoxey[38], the measured pressure coefficient,  $-0.25$ , falls within one standard deviation of the mean calculated pressure coefficient at the windows,  $-0.27 \pm 0.10$ . Furthermore, in order for flow to move across

the length of the greenhouse from the windows downwind to windows upwind, a gradient in the pressure distribution over the windows is necessary. A constant pressure distribution determined by Wells and Hoxey is not an accurate estimation.

While these measurements have been widely used for CFD ventilation calculation validation, it is also important to note that the values are intended for predicting structural stability of greenhouses due to wind loading.

## 5-3 Results

Following the verification and validation, this section presents a discussion of the resulting flow patterns of the 'constant' case. None of the variable cases will be evaluated due to the inability to verify the results.

### Flow Field

The following figures present the latest time step calculated for a plane perpendicular to the greenhouse ridges located along the windward window openings. Figure 5-20 shows flow separation occurring, with a clear boundary layer over the greenhouse. Introducing the greenhouse with its pitched roofs and window flaps into the flow alters the structure of the boundary layer near the ground, increasing wall shear stress and skin friction.

This plot also indicates the flow within the greenhouse is opposite to the flow in the external environment, flowing from right to left within the greenhouse, and from left to right outside the greenhouse. Figures 5-20 and 5-22 both show air entering through the vents downwind and near the center of the greenhouse, while wind exits through upwind vents. There still exists both inflow and outflow in each window. The  $z$  velocity plot shows the very first window having much higher inflow and outflow magnitudes when compared with the other windward facing windows in the contour plot.

The  $y$  component of velocity presented in Figure 5-21 shows low velocities across the width of the greenhouse. As expected,  $y$  velocities are very low, yet present due to the influence of the staggered leeward-facing windows which act as an outlet to the windward-facing velocity field presented in the figure.

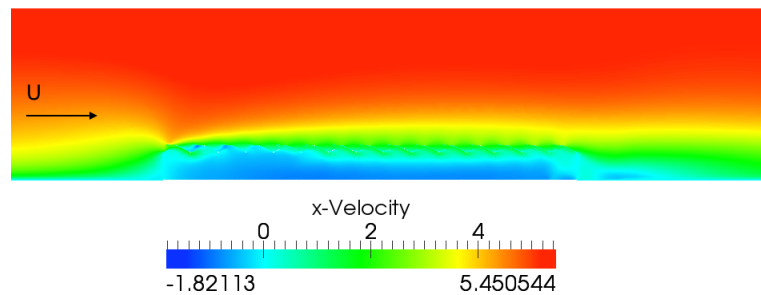


**Figure 5-20:**  $x$  component of velocity flow field [ $m/s$ ] for the 'constant' simulation

The vector plot colored according to velocity magnitude in Figure 5-23 provides more insight into the velocities in the  $y$  direction. The figure shows the velocity at a plane (a) 1 meter and (b) 3.7 meters from the floor of the greenhouse (1 meter below the midpoint of the windows). Vectors are oriented based on velocity direction. In both figures, the highest velocities occur near the walls.

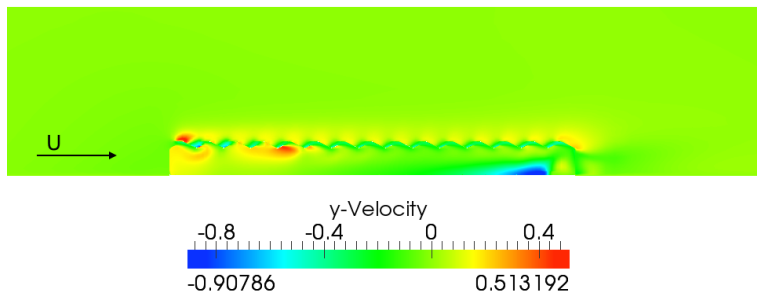


**Figure 5-21:**  $y$  component of velocity flow field [ $m/s$ ] for the 'constant' simulation

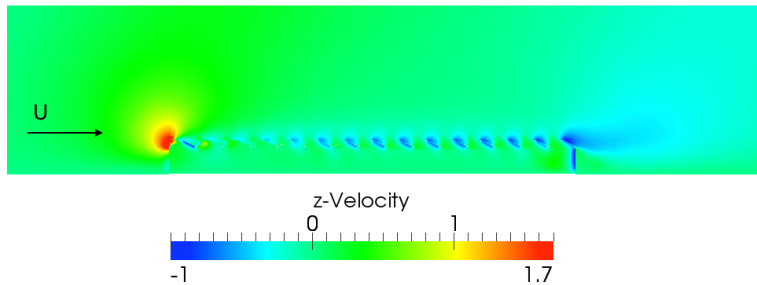


**Figure 5-22:**  $z$  component of velocity flow field [ $m/s$ ] for the 'constant' simulation

In addition to internal flow moving opposite to the external wind direction, vortices can be seen in the corners of the greenhouse near the floor. There is a slightly diagonal flow pattern across the greenhouse.

Closer to the windows, in Figure 5-23(b), the influence of the window direction on the flow patterns within the greenhouse can be seen. Velocities just below windward facing windows generally point in the  $+x$  direction (particularly at the downwind end of the greenhouse), while near the leeward facing windows the flow generally is directed upwind inside the greenhouse (particularly near the center span of the greenhouse). Flow near the leeward-facing windows, however, is less consistent with regard to direction, indicating turbulent flow activity in these regions. The large vortices on the windward side of the greenhouse extend over the height of the greenhouse, spanning from the floor to the region just below the windows. These vortices occur as a result of flow directed towards the edges as it enters the first row of windward facing windows, and flow directed to the center of

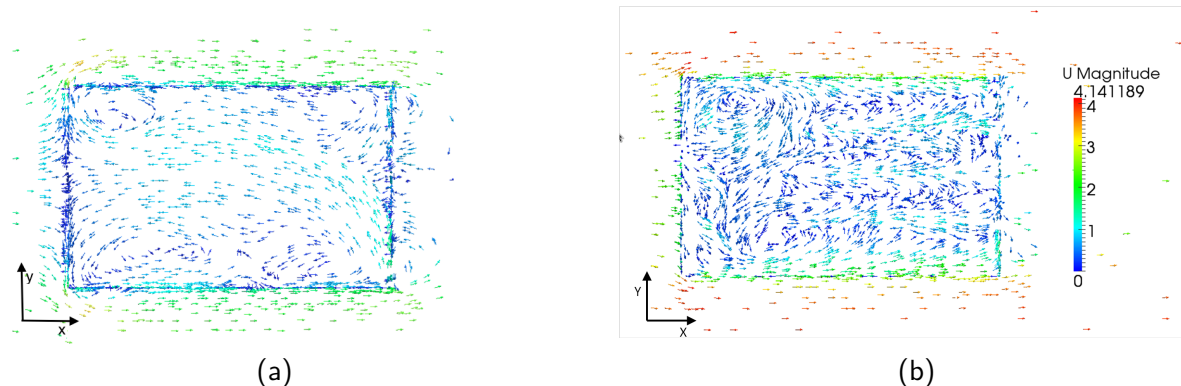


**Figure 5-23:** Velocity vector field at a plane parallel to the ground located (a) 1 meter from the ground and (b) 3.7 meters from the ground, colored by velocity magnitude [ $m/s$ ]

the greenhouse at windward facing windows along the edges.

### Window Fluxes

A closer look at the flux through the windows of the 'constant' case can provide further detail about the greenhouse ventilation. Figure 5-24 presents the volumetric flow rate at the windows of the 'constant' case.

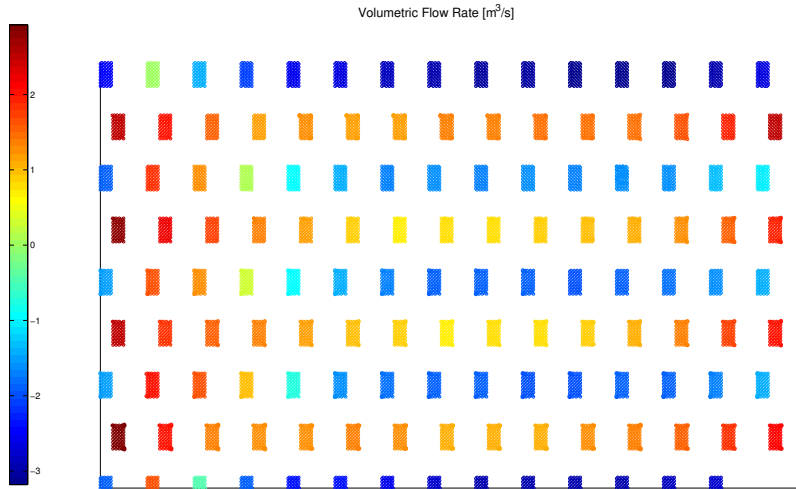


**Figure 5-24:** Volumetric flow rate at windows of the 'constant' case in  $m^3/s$

With wind moving in the  $+x$  direction, the windward facing windows of the first span where the wind first interacts with the building shows a very high volumetric inlet flow rate and the corresponding leeward facing windows on the span show high outlet rates. The windward facing windows have a pattern of initial high volumetric inlet flow rate at the first span followed by a net air outlet from the windward facing windows upwind. From the center to the downwind spans, the inlet flow rate gradually increases through the windward facing windows. The air inlet rate is also unusually high on the edges of the span, while the leeward facing windows show a initial high outflow rate, followed by a decrease in outflow towards the center and increase in outflow rates at the downwind leeward facing windows.

Over the latest 30 seconds of stabilized computation time, the time-averaged velocity magnitude through the windows, normalized by the free stream velocity at the window height ranged from 2.76E-3 to 1.12, averaging 0.60. The standard deviations of the velocity vector components gives an indication of turbulence effects. Standard deviations for the  $x$ ,  $y$ , and  $z$  components averaged 4.82E-3, 4.25E-3, and 1.69E-3, respectively.

(

Pressure Field)

The pressure plot in Figure 5-25 shows the stagnation point, where the free flowing wind first meets the greenhouse at the left side. The very small pressure difference across the length of the greenhouse induces the flows from high to low pressure (in the  $-x$  direction) observed in the velocity plots. Furthermore, despite the generally higher pressure within the greenhouse, the pressures along the outside of the roof adjacent to windows where air enters the greenhouse are higher than the pressures inside the greenhouse, inducing flow into the greenhouse.

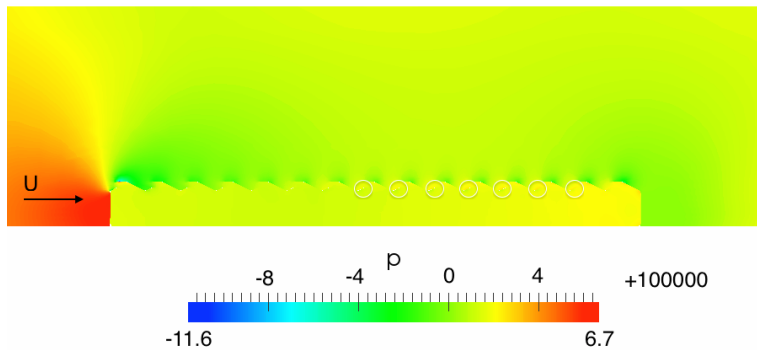


**Figure 5-25:** Pressure field of the 'constant' simulation ( $p/\rho$  [ $m^2/s^2$ ]). White circles identify a pressure difference between the inside and outside of the greenhouse, driving airflow into the greenhouse

### Turbulence Properties

The turbulent kinetic energy depicted in Figure 5-26 indicates there are large velocity fluctuations at the first two spans of the greenhouse, where the wind first interacts with the structure. The low turbulent kinetic energy within the greenhouse indicates fairly stable flow within the greenhouse, with the largest effect occurring as a result of the roof spans and window flaps.

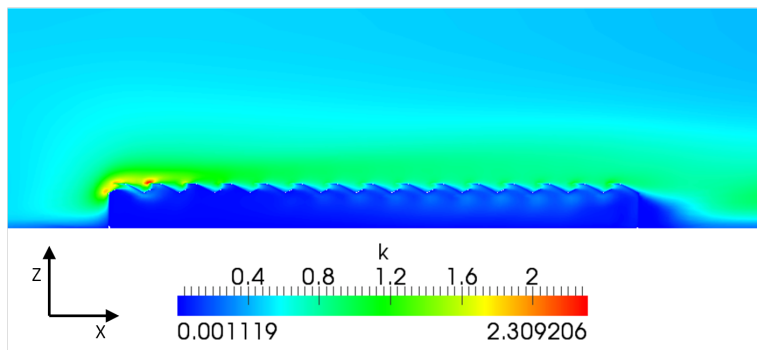


**Figure 5-26:** Results for turbulent kinetic energy field

The turbulent kinetic energy dissipation, in Figure 5-27, is also fairly high at the front edges of the greenhouse, preventing the turbulent fluctuations from spreading far beyond this region. A high turbulent kinetic energy dissipation is expected in regions with higher velocities (and resulting kinetic energy) and smaller turbulent eddy length scales.

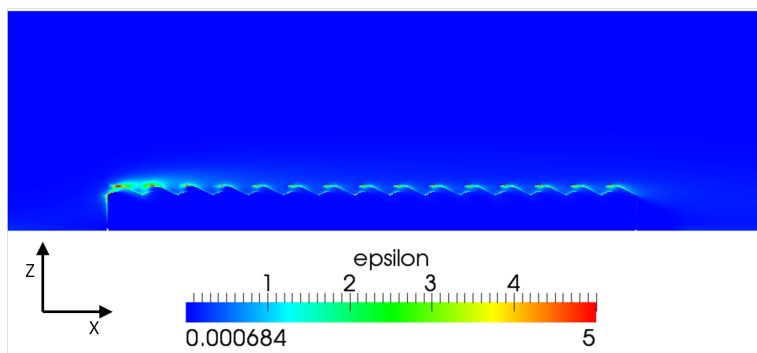


**Figure 5-27:** Turbulent kinetic energy dissipation field for the 'constant' case

---

# Chapter 6

---

## Boundary Analysis

While errors in the initialization of variable simulations prevent further analysis in this work, this section presents a discussion of how valid and verified results could be used to formulate a greenhouse ventilation boundary condition. The methodology for developing a boundary condition can be broken down into two steps: First, an analysis of which parameters must be assigned to the ventilation boundary of an internal greenhouse CFD calculation is needed in order to maintain a stable simulation and produce a physically meaningful result. Next, the assigned values for the selected parameters are determined based on the results of the test calculations.

### 6-1 Selecting parameters

When calculating flows in a greenhouse as incompressible and neglecting the effects of buoyancy, the modeled parameters are pressure (normalized by density,  $m^2/s^2$ ), velocity, turbulent kinetic energy, and turbulent kinetic energy dissipation. It is not necessary to prescribe values for all parameters, as this can over-constrain the calculation. For example, pressure and velocity are coupled in the momentum equation. Therefore it is necessary to prescribe one of the two values at a boundary. Given that velocity is a vector of three components, and pressure is a scalar, pressure is the ideal parameter of the two to prescribe at the boundary. Furthermore, the continuity equation requires the net flux in and out of the greenhouse to be zero. The pressure and velocity boundary conditions must not over constrain this requirement. Turbulent eddies are present at the windows, requiring turbulence properties to be specified at the boundary as well. Turbulent kinetic energy, turbulent kinetic energy dissipation, and velocity are also interrelated, and it is therefore not possible to prescribe all three at a single boundary.

Several tests investigated the parameters to be implemented at the boundary of an internal greenhouse model using the mapped values from the CFD simulation results. With pressure driven flow being the most ideal, two dimensional tests were initially simulated to determine whether a boundary condition was feasible before adding the complexity of 3-dimensionally staggered greenhouse windows. Three pressure boundary options were tested in a simplified two-dimensional calculation containing two windows:

- A "pressure directed inlet velocity" boundary condition determines velocity based on static pressure and a specified velocity direction vector
- Static pressure

- Total pressure

The "pressure directed inlet velocity" is less ideal for a boundary condition, because it requires the specification of a velocity direction vector in addition to the static pressure (four components altogether). The most stable calculation resulted in a combination of total pressure at the inlet boundary face and static pressure prescribed at the outlet boundary face. However, testing this combination of boundary conditions for internal flow of a greenhouse using mapped pressure values (from an external environment calculation) resulted in an unstable calculation. This test was unstable because of the complexity of introducing 134 windows distributed over a greenhouse roof in three dimensions.

Prescribing velocity over the window boundaries was also not possible, because continuity (Equation 2-9) must be satisfied. The prescribed velocity must be very accurate. Even a small roundoff error can easily prevent continuity from being achieved. Therefore, as is common practice in Computational Fluid Dynamics (CFD) calculations, a combination of velocity and pressure were prescribed at the boundaries of the internal greenhouse model.

In general, pressure is prescribed at an outlet, and velocity at the inlet. However, most of the windows act as both an inlet and outlet. Several combinations of pressure and velocity boundaries were simulated to determine the optimal combination. It was determined that the calculation is less stable when pressure is prescribed on the majority of windows because flow direction is only specified for a single window. With this in mind, the following two configurations were tested:

- Pressure prescribed at a single window and velocity prescribed at all other windows;
- Pressure prescribed at four windows which act as a net outlet and velocity prescribed at all other windows;

The internal flows that result from these mapped calculations give similar results to the initial calculations which simulate the entire external environment. However, large errors exist in both cases. Recalling back to the flux analysis of the constant case, there was a very large unphysical net inflow into the greenhouse of  $14.2 \text{ m}^3/\text{s}$ . This large inflow is also captured when the velocities at the windows were interpolated to the closed greenhouse model. In order to satisfy continuity, the window(s) in which velocity is not fixed must correct for the large inflow. In the first case, when the pressure is prescribed at a single window, an extreme outlet velocity is observed. The second case, in which pressure is prescribed at four net outlet windows resulted in larger errors at the downwind side of the greenhouse, where the pressure boundaries were specified. A conclusion of the two tests is that the pressure inlet windows should be selected according to the desired error distribution.

The figures below show the two tests that determine where the ideal pressure prescribed window should be located. The middle row of Figure 6-1 identifies a window which behaves mostly as an inlet, while the bottom row identifies four leeward-facing windows that act mostly as outlets. The results show that the inlet window becomes an outlet with a very high velocity, while the outlet window selections remain outlets, but simulate a higher velocity than expected. Furthermore, the pressure within the greenhouse increases for a pressure prescribed on an inlet window, while the pressure decreases within the greenhouse when the pressure is prescribed on the outlet windows.

With the goal of replicating the internal flows, the internal flows are shown in Figures 6-2 and 6-3. The velocity flows and pressure distribution for the slide single inlet pressure specification are as expected, while large errors appear to be present when pressure was specified on the selection of four outlet (leeward-facing) windows. It is important to note that despite different pressures within the greenhouse, the distribution remains the same for the single window pressure prescription, resulting in the same velocity field as expected.

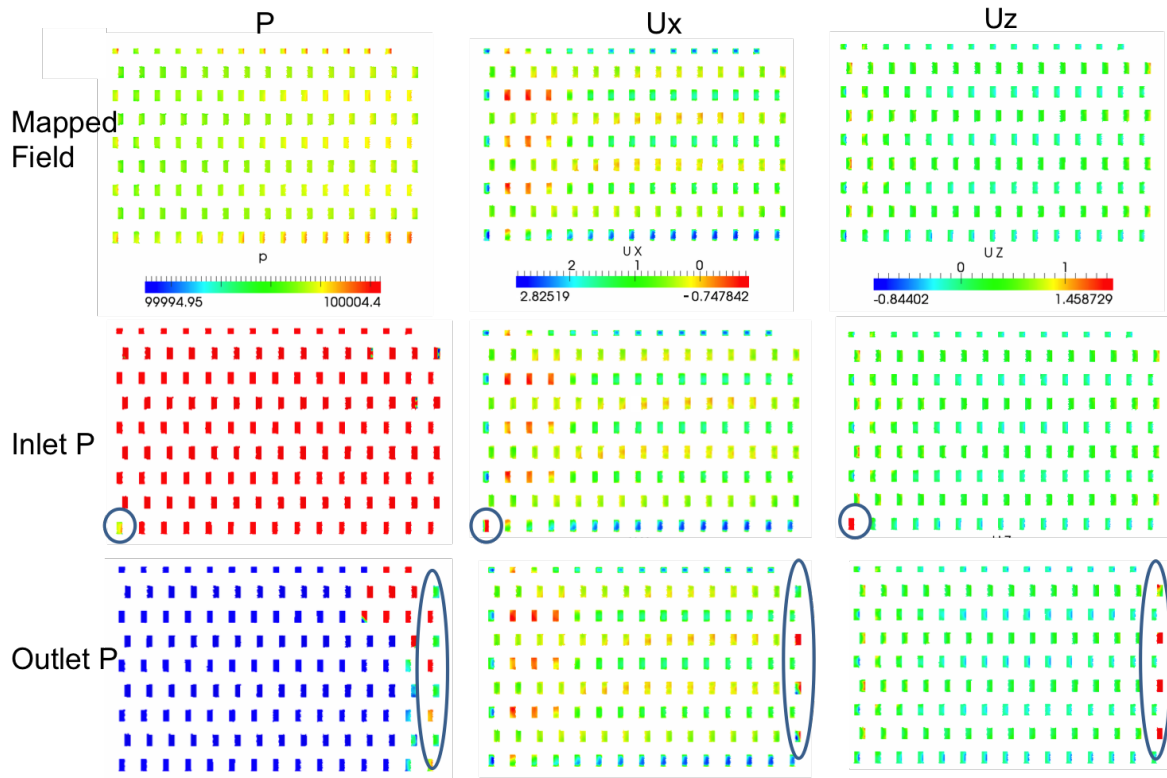


**Figure 6-1:** Selecting boundary condition parameters: two tests show the results of prescribing a mapped (top row) pressure on a single window (middle row) or selection of windows (bottom row), while velocity is prescribed on all others

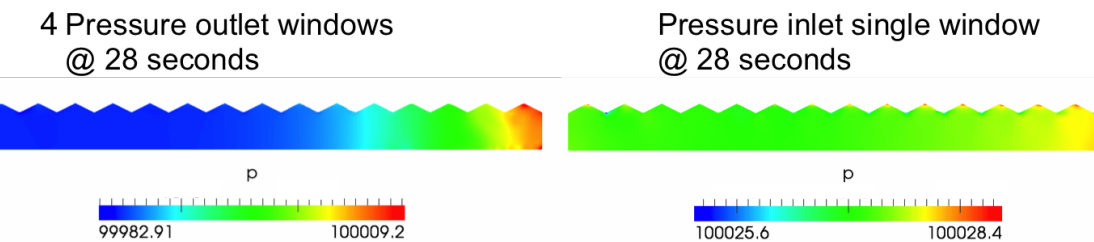
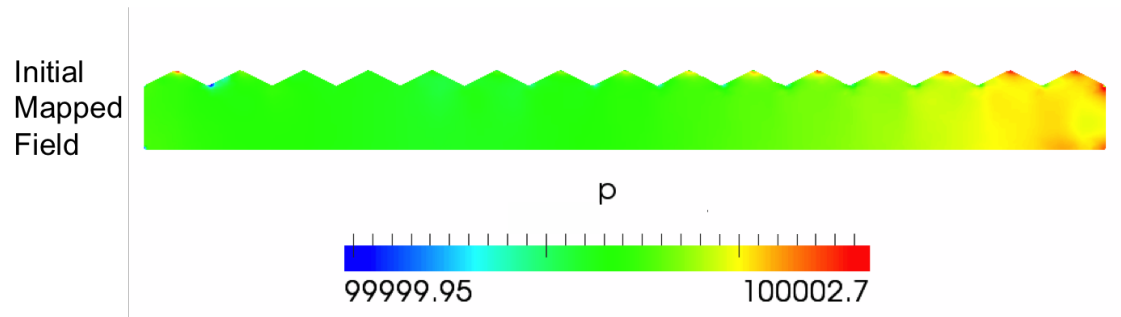


**Figure 6-2:** Selecting boundary condition parameters: Results of prescribing a mapped (top) pressure on a single window (middle row) or selection of windows (bottom row), while velocity is prescribed on all others

Despite the similarities in the flows shown for prescribing the pressure at the single window, there remains high errors near the window. However, the other test produced errors in the vicinity of all four pressure-prescribed windows. To minimize this error, different numerical schemes were

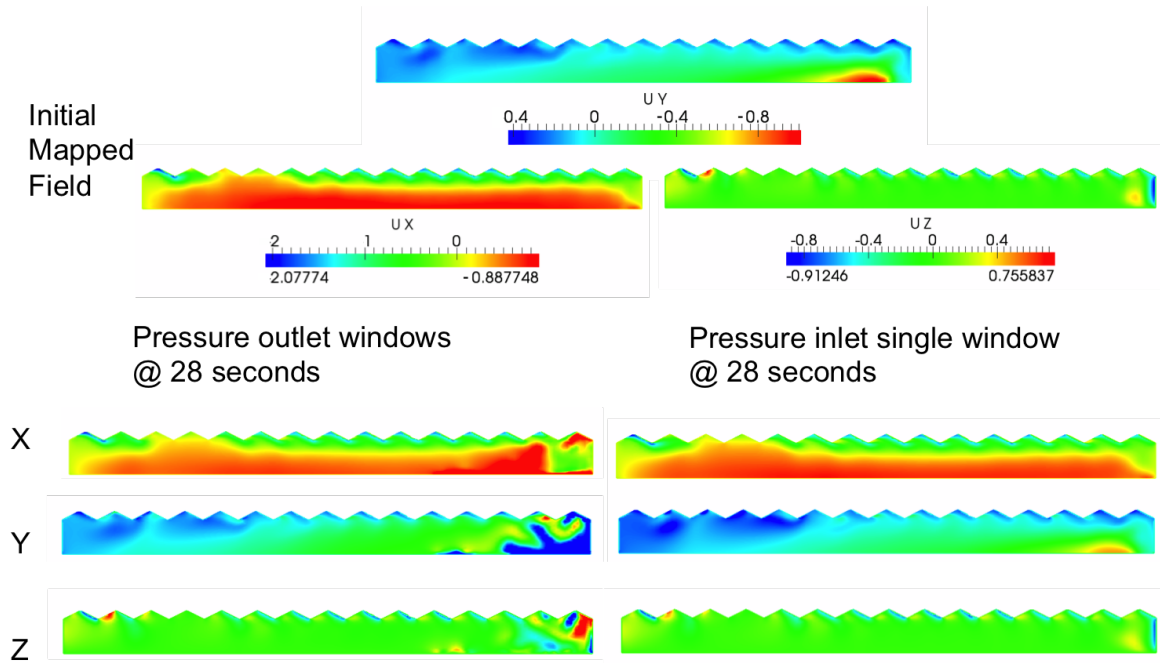


**Figure 6-3:** Selecting boundary condition parameters: results of prescribing a mapped (top) pressure on a single window (middle row) or selection of windows (bottom row), while velocity is prescribed on all others

tested (additional non-orthogonal correctors and higher order gradient schemes), as well as different boundary condition types (i.e. 'pressure directed inlet velocity', static pressure, and total pressure). Specifying the direction of the velocity at the pressure-prescribed boundary, for example, appears not to satisfy continuity.

Tests were also done to determine that optimal results occur when both turbulent kinetic energy and turbulent kinetic energy dissipation are prescribed at all boundaries.

## 6-2 Parameter value specification

The complex air exchanges that occur between the staggered windward and leeward windows requires a simplified method for predicting and prescribing boundary conditions at the windows.

There are two options for specifying parameters at the ventilation boundary condition. The first option interpolates measurements of the test calculations to generate an estimation of the boundary conditions for a specified window opening angle and wind azimuth angle. This option does not provide flexibility with respect to the greenhouse geometry and window geometries. The second option develops trends using regression analysis to determine the estimated ventilation boundary condition. This option has the potential of applying for a wider range of greenhouse geometries. Both options are investigated in this study.

### 6-2-1 Interpolation

Interpolation of the boundary condition is done by sampling the boundary fields of external flow simulations with slightly larger and slightly smaller window opening angles, and using these interpolated values to prescribe the boundary conditions of an internal greenhouse flow calculation. This

method makes the assumption that a linear trend exists between the boundary conditions in two simulations of window opening angle, which was not observed to realistically portray the window opening trends, according the multiple regression analysis in the following section.

### 6-2-2 Multiple regression analysis

Multiple regression analysis is used to fit data to a trend and determine the relationship between dependent (response) variables and independent (predictor) variables. In this case, a multiple regression analysis is performed for each of the boundary variables, as well as for the pressure coefficient difference when comparing the value at an open window to a closed window. The pressure and velocity response variables are analyzed as non-dimensional variables, in order to scale boundary values according to different wind velocities and outdoor pressure conditions. A stepwise method can be used to determine statistically significant relations and interactions of predictor variables. This method, available in the Matlab statistics toolbox, begins with an assumed trend (i.e. constant, quadratic) between the predictor and response variables, along with interaction terms among the predictor variables. The method iteratively removes (or adds in the case of a constant base trend) coefficients that are insignificant according to the p-value discussed in the stationarity test in the previous chapter, and recalculates the coefficients until all remaining terms are statistically significant.

Five predictor variables to be assessed:

- Span number (a categorical version of  $x$ -coordinate)
- Y-coordinate
- Height ( $z$ -coordinate)
- window direction (leeward-facing or windward-facing)
- windward window area
- leeward window area

Span number was selected because it is typical for pressure distribution over a greenhouse to be determined according to the span number. Furthermore, for greenhouses with many spans, central spans often exhibit the same behavior, making it easier to match this model to other greenhouse geometries. With the window plane at a tilt, there is a strong correlation between the fixed  $x$  and  $z$  coordinates of points in the window boundary. There is furthermore a correlation between the  $x$  coordinate and window direction, which alternates along the  $x$  axis. Therefore, the  $x$ -coordinate is represented as the categorical "Span number" predictor variable, which eliminates these dependencies. The  $z$ -coordinate is expected to indicate trends over the height of each individual window. The observed inlet and outlet tendencies of the window flux in Figure 5-24 suggest that window direction is a significant nominal variable to test.

The reported results from literature has shown strong trends in window direction as well as significance of window angle. Window direction is to be represented as a nominal predictor, generating a separate trend for leeward and windward facing windows. Stronger regression models can be produced using the effective window area in comparison to window opening angle, as expected, given that ventilation rates are directly proportional to vent area. The effective window area is calculated as

$$A = W \sqrt{2L^2(1 - \cos(\alpha)) + L^2 \sin(\alpha)} \quad (6-1)$$

where  $L$  is the length of the window,  $W$  is the width of the window (along the width of the greenhouse), and  $\alpha$  is the window opening angle from the plane of the greenhouse roof. A similar technique was used by Bailey et. al. [39] to determine the effect of window opening angles on ventilation rate.

Assuming Reynolds independence, a common assumption used in wind engineering, the effect of different wind speeds can be determined by scaling the velocity. Therefore, the non-dimensional velocities should be modeled in the regression analysis.

Given the concurrent initiative to develop a "Cp Generator" at TNO, which estimates the pressure distribution over the roof and walls of various building geometries (without windows), a regression model can also be developed for the pressure coefficient *difference* that results from opening windows along the surface of the greenhouse geometry.

---

# Chapter 7

---

## Recommendations

While it is unfortunate that the variable simulations of window opening angles and wind directions were not verifiable, many lessons were learned that can further improve the implementation of these calculations in future work. These simulations can be improved by ensuring the wall boundary conditions are unchanged during initialization. Furthermore, the linear solvers can be updated using the suggestions in Section 4-2-1 to speed up the calculations. Other forms of initialization are also possible, such as beginning the calculation on a coarser mesh before mapping the results to the finer mesh, or using the PotentialFoam solver to generate the starting fields for the full Navier-Stokes PisoFoam solver.

Simulations of other external parameters that influence ventilation (identified in Section 3-1) can greatly improve this work. Looking back on the work, it would be beneficial to find a correlation between greenhouse geometry and ventilation as well. Or at the very least, implement these boundary conditions on a greenhouse with different geometry and validate the results.

A possibility for improving the calculations further would be the much more computationally expensive Large Eddy Simulation (LES) methodology, using a simplified greenhouse geometry. This method may more accurately model the external and internal greenhouse flow given the range of turbulence length scales that are limited when using the Reynolds Averaged Navier-Stokes (RANS) methodology.

Validation of the simulations using either experimental velocity values for various window opening angles or in a controlled wind tunnel simulation would improve the confidence in the various window opening angle simulations.

Implementation of the boundary condition and the accuracy of such simulations are highly dependent on the configuration of pressure and velocity boundaries. A solution to this problem could be to alter the solver so that it distributes the concentration of error (correcting for continuity) that presently only exists at the pressure boundary.



---

# Chapter 8

---

## Conclusion

This graduation project focussed on developing a ventilation boundary condition for a horticultural greenhouse climate model with the goal of replicating the internal flows of the greenhouse. The selected boundary condition variables were window opening angle and wind direction. The method used to develop this boundary condition was through simulation of these variables in an external flow environment using Reynolds Averaged Navier-Stokes (RANS) turbulence modeling. A thorough verification of the resulting simulations examined spatial convergence, temporal convergence, model implementation, iterative convergence, and consistency.

The results of the wind azimuth angle simulations were found to not yet be completely converged. Evidence of this included negative pressure force for one of the simulations, high residual error, failure of a statistical stationarity test, and strong correlations between the initialized conditions and final values. However, while the results of varied window opening angles reached reasonable convergence, they failed to satisfy continuity, leading to the further conclusion that initialization errors were also present in these simulations.

The resulting flows for the constant case were consistent with qualitative flow trends reported in other greenhouse studies. Flow typically enters through the downwind windows and exits through upwind windows. This flow behavior also induced large eddies in the corners of the greenhouse near the windward side. The pressure distributions of this case were validated using Wells and Hoxey's experimental pressure distributions [38]. A valid pressure distribution indicates that the pressure-induced ventilation calculations should also be accurate.

The complexity of an internal greenhouse Computational Fluid Dynamics (CFD) model due to the extensive window layout required boundary specifications of both pressure and velocity at different greenhouse windows. Various configurations were tested for pressure and velocity specification along the greenhouse ventilation boundary faces, resulting in concentrated error near the pressure-prescribed windows. With more pressure-prescribed windows, the erroneous flow was less extreme, distributed among the windows.

Two methods, interpolation and regression analysis, were discussed as methods for implementing a boundary condition at the greenhouse windows. Regression modeling can be used to predict pressure and velocity distributions using the span number (an ordinal variable),  $y$  position, height ( $z$  position), window direction, and effective windward and leeward window opening areas. This method has the potential to eventually provide more flexibility in greenhouse geometry.

While errors were present when implementing a boundary condition for the 'constant' case, there remains the benefit that reasonable internal flow may be simulated without the computational cost and

time of simulating the entire external environment. Approximate solutions obtained with numerical methods inherently contain discretization and modeling errors. When compared to ventilation calculations in an operational greenhouse, uncertainties and errors are unavoidable in such uncontrolled environments. Therefore, for the purpose of estimating the general flows within a greenhouse, this model is sufficient. When monitoring the climate at a precise location (rather than a general region in the greenhouse) and when using model values for climate control applications, a more accurate measurement is necessary. Further improvements are needed for applications requiring more accurate estimates of flow within the greenhouse.

---

---

## Appendix A

---

### **Appendix: Boundary Conditions**

	<b>Velocity, <math>\mathbf{U}</math></b>	<b>Pressure, <math>\mathbf{p}</math></b>	<b>Turbulent Kinetic Energy, <math>k</math></b>	<b>Turbulent Kinetic Energy Dissipation, <math>\epsilon</math></b>
<b>Dimensions</b>	$m/s$	$m^2/s^2$	$m^2/s^2$	$m^2/s^3$
Greenhouse Floor	fixedValue (0 0 0)	zeroGradient	kqRWallFunction	epsilonWallFunction
Greenhouse Ceiling	fixedValue (0 0 0)	zeroGradient	kqRWallFunction	epsilonWallFunction
Greenhouse Walls	fixedValue (0 0 0)	zeroGradient	kqRWallFunction	epsilonWallFunction
Atmosphere	zeroGradient	zeroGradient	zeroGradient	zeroGradient
Surroundings	zeroGradient	zeroGradient	zeroGradient	zeroGradient
Earth	fixedValue (0 0 0)	zeroGradient	kqRWallFunction	epsilonWallFunction
Inlet	atmBoundaryLayerInletVelocity	zeroGradient	fixedValue 0.50497	atmBoundaryLayerInletEpsilon
Outlet	inletOutlet	fixedValue 100000	zeroGradient	zeroGradient

**Table A-1:** Boundary conditions

---

## Appendix B

---

# Appendix: Calculation Details

### Finite Volume Calculation Schemes

```
1  /*-----*-- C++  
2  *-----*\\  
3  | \\\      / F ield          | OpenFOAM: The Open Source CFD Toolbox  
4  | \\\      / O peration       | Version: 2.2.0  
5  |   \\\  / A nd            | Web:      www.OpenFOAM.org  
6  |   \\\ / M anipulation    |  
7  *\-----*/  
8 FoamFile  
9 {  
10    version      2.0;  
11    format        ascii;  
12    class         dictionary;  
13    object         fvSchemes;  
14 }  
15 // * * * * * * * * * * * * * * * * * * * * * * * * * * * * * * * * * * * * * * * * * * * *  
16 * */  
17 ddtSchemes  
18 {  
19     default      backward;  
20 }  
21  
22 gradSchemes  
23 {  
24     default      Gauss linear;  
25 }  
26  
27 divSchemes  
28 {  
29     default      none;
```

```

30     div(phi,U)           Gauss limitedLinearV 1.0 phi;
31     div((nuEff*dev(T(grad(U)))))   Gauss linear;
32     div(phi,epsilon)    bounded Gauss linear;
33     div(phi,k)         bounded Gauss linear;
34 }
35
36 laplacianSchemes
37 {
38     default            Gauss linear limited corrected 0.333;
39 }
40
41 interpolationSchemes
42 {
43     default            linear;
44 }
45
46 snGradSchemes
47 {
48     default            limited corrected 0.333;
49 }
50
51 fluxRequired
52 {
53     default            no;
54     p;
55 }
56
57
58 //*****
//*****

```

### Finite Volume Solution Methods

```

1 /*-----*-- C++
-----*/
2 | ====== |
3 | \\      / F ield          | OpenFOAM: The Open Source CFD Toolbox
4 | \\      / O peration       | Version: 2.2.0
5 | \\  / A nd              | Web:      www.OpenFOAM.org
6 | \\\ M anipulation | |
7 \*-----*/
8 FoamFile
9 {
10     version      2.0;
11     format       ascii;
12     class        dictionary;
13     object       fvSolution;
14 }
15 // * * * * *
* */
16

```

```

17 solvers
18 {
19     p
20     {
21         solver          PCG;
22         preconditioner DIC;
23         tolerance      1e-06;
24         relTol         0;
25     }
26
27     pFinal
28     {
29         solver          PCG;
30         preconditioner DIC;
31         tolerance      1e-06;
32         relTol         0;
33     }
34
35     U
36     {
37         solver          smoothSolver;
38         smoother        GaussSeidel;
39         tolerance      1e-8;
40         relTol         0.1;
41         nSweeps        1;
42     }
43
44     k
45     {
46         solver          smoothSolver;
47         smoother        GaussSeidel;
48         tolerance      1e-8;
49         relTol         0.1;
50         nSweeps        1;
51     }
52
53     epsilon
54     {
55         solver          smoothSolver;
56         smoother        GaussSeidel;
57         tolerance      1e-8;
58         relTol         0.1;
59         nSweeps        1;
60     }
61 }
62
63 PISO
64 {
65     nCorrectors      3;
66     nNonOrthogonalCorrectors 1;
67     pRefCell        0;
68     pRefValue       0;
69 }
70
71
72 // ****
// 
```



---

# Bibliography

- [1] M. Peet and G. Welles, "Greenhouse tomato production," in *Tomatoes* (E. Heuvelink, ed.), vol. 13 of *Crop Production Science in Horticulture*, pp. 257–304, Wallingford, Oxfordshire OX10 8DE, UK: CABI Publishing, 2005.
- [2] W. Baltussen, "Greenhouse technology suppliers conquer the world," Survey results of AVAG Plus members 13-008, LEI Wageningen UR, Wageningen, March 2013.
- [3] P.-E. Bournet, "Assessing greenhouse climate using CFD: a focus on air humidity issues," tech. rep., Agrocampus Ouest, Angers, France, 2013.
- [4] P.-E. Bournet, S. Ould Khaoua, T. Boulard, C. Migeon, and G. Chassériaux, "Effect of roof and side opening combinations on the ventilation of a greenhouse using computer simulation," *Transactions of the ASABE*, vol. 50, no. 1, pp. 201–212, 2007.
- [5] T. Bartzanas, T. Boulard, and C. Kittas, "Effect of vent arrangement on windward ventilation of a tunnel greenhouse," *Biosystems Engineering*, vol. 88, no. 4, pp. 479–490, 2004.
- [6] T. Boulard, H. Fatnassi, A. Kichah, F. Girardot, J. C. Roy, and I. B. Lee, *Development and validation of a global CFD model of heat, water vapour and fungal spores transfers in a greenhouse*, vol. 801 PART 2 of *Acta Horticulturae*. 2008. Cited By (since 1996):1.
- [7] E. Romano, F. Nucci, and C. Bisaglia, "A theoretical approach for a sensitive analysis of the influences of external factors on greenhouse microclimate," *Acta Horticulturae*, vol. 919, pp. 81–88, 2011. cited By (since 1996)0.
- [8] G. Bot, *Greenhouse climate: from physical processes to a dynamic model*. PhD thesis, Wageningen University, 1983. cited By (since 1996)1.
- [9] J. de Jong, *Natural ventilation of large multi-span greenhouses*. PhD thesis, Wageningen University, 1990. cited By (since 1996)73.
- [10] A. Mistriotis, G. Bot, P. Picuno, and G. Scarascia-Mugnozza, "Analysis of the efficiency of greenhouse ventilation using computational fluid dynamics," *Journal of Agricultural Engineering Research*, vol. 85, pp. 217–228, 1997.
- [11] T. Boulard and A. Baille, "Modelling of air exchange rate in a greenhouse equipped with continuous roof vents," *Journal of Agricultural Engineering Research*, vol. 61, no. 1, pp. 37–48, 1995.

- [12] P.-E. Bournet and T. Boulard, "Effect of ventilator configuration on the distributed climate of greenhouses: A review of experimental and CFD studies," *Computers and Electronics in Agriculture*, vol. 74, no. 2, pp. 195 – 217, 2010.
- [13] M. Teitel, G. Ziskind, O. Liran, V. Dubovsky, and R. Letan, "Effect of wind direction on greenhouse ventilation rate, airflow patterns and temperature distributions," *Biosystems Engineering*, vol. 101, pp. 351–369, 2008.
- [14] H. Fatnassi, T. Boulard, C. Poncet, and M. Chave, "Optimization of greenhouse insect screening with computational fluid dynamics," *Biosystems Engineering*, vol. 93, pp. 301–312, 2006.
- [15] S. Ould Khaoua, P. Bournet, and G. Chassériaux, "Mathematical modelling of the climate inside a glasshouse during daytime including radiative and convective heat transfers," *Acta Horticulturae*, vol. 718, pp. 255–262, 2006. cited By (since 1996)1.
- [16] S. Reichrath and T. Davies, "Using CFD to model the internal climate of greenhouses: Past, present and future," *Agronomie*, vol. 22, no. 1, pp. 3–19, 2002. cited By (since 1996)65.
- [17] J. Ferziger and M. Peric, *Computational Methods for Fluid Dynamics*. Springer-Verlag, third ed., 2002.
- [18] H. Versteeg and W. Malalasekera, *An introduction to computational fluid dynamics: The finite volume method*. Longman Group, 1995.
- [19] C. Rhie and W. Chow, "Numerical study of the turbulent flow past an airfoil with trailing edge separation," *AIAA Journal*, vol. 21, no. 11, pp. 1525–1532, 1983.
- [20] F. P. Kärrholm, "Rhie-Chow interpolation in OpenFOAM," tech. rep., Chalmers University of Technology, Göteborg, Sweden, 2006.
- [21] R. Issa, "Solution of the implicitly discretized fluid flow equations by operator-splitting," *Journal of Computational Physics*, vol. 62, pp. 40–65, 1986.
- [22] H. kan Nilsson, "A look inside icofoam (and pisofoam)," Presented at the MSc/PhD course in CFD with OpenSource software, 2013.
- [23] H. Jasak, *Error analysis and estimation for the finite volume method with applications to fluid flows*. PhD thesis, Imperial College London, 1996.
- [24] Y. Jiang and Q. Chen, "Study of natural ventilation in buildings by large eddy simulation," *Journal of Wind Engineering and Industrial Aerodynamics*, vol. 89, no. 13, pp. 1155–1178, 2001.
- [25] B. Launder and D. Spalding, "The numerical computation of turbulent flows," *Computer Methods in Applied Mechanics and Engineering*, vol. 3, no. 2, pp. 269–289, 1974.
- [26] T.-H. Shih, W. Liou, A. Shabbir, Z. Yang, and J. Zhu, "A new  $k-\epsilon$  eddy-viscosity model for high reynolds number turbulent flows - model development and validation," *Computers Fluids*, vol. 24, no. 3, pp. 227–238, 1995.
- [27] KNMI, "Climatology: Daily weather data of the netherlands," May 2014.
- [28] "Gnu general public license, version 3." <http://www.gnu.org/licenses/gpl.html>, June 2007. Last retrieved 2012-05-10.
- [29] "Blatt 9: 2005-11, umweltmeteorologie - prognostische mikroskalige windfeldmodelle - evaluierung für gebäude- und hindemisumströmung, beuth," 2005. cited By (since 1996)1.

- [30] B. Blocken, S. Roels, and J. Carmeliet, "Modification of pedestrian wind comfort in the silvertop tower passages by an automatic control system," *Journal of Wind Engineering and Industrial Aerodynamics*, vol. 92, no. 10, pp. 849–873, 2004.
- [31] T. Wintergerste, M. Casey, and A. Hutton, "The best practice guidelines for CFD - a european initiative on quality and trust," in *American Society of Mechanical Engineers 2002 Pressure Vessels and Piping Conference*, vol. 448, pp. 1–9, 2002. cited By (since 1996)1.
- [32] P. Richards and R. Hoxey, "Appropriate boundary conditions for computational wind engineering models using the k-epsilon model," *Journal of Wind Engineering and Industrial Aerodynamics*, 1993.
- [33] J. W. Slater, "Nparc alliance cfd verification and validation." <http://www.grc.nasa.gov/WWW/wind/valid/>, March 2012. Last retrieved 2014-08-10.
- [34] T. Norton, D.-W. Sun, J. Grant, R. Fallon, and V. Dodd, "Applications of computational fluid dynamics (CFD) in modelling and design of ventilation systems in the agricultural industry: A review," *Bioresource Technology*, vol. 98, no. 12, pp. 2386–2414, 2007.
- [35] S. Wang and J. Deltour, "Lee-side ventilation-induced air movement in a large-scale multi-span greenhouse," *Journal of Agricultural Engineering Research*, vol. 719, pp. 103–110, 1999.
- [36] T. Boulard, G. Papadakis, C. Kittas, and M. Mermier, "Air flow and associated sensible heat exchanges in a naturally ventilated greenhouse," *Agricultural and Forest Meteorology*, vol. 88, pp. 111–119, 1997.
- [37] A. Mistriotis, T. de Jong, M. Wagemans, and G. Bot, "Computational fluid dynamics (cfd) as a tool for the analysis of ventilation and indoor microclimate in agricultural buildings," *Netherlands Journal of Agricultural Science*, vol. 45, pp. 81 – 96, 1997.
- [38] D. Wells and H. Hoxey, "Measures of wind loads on full-scale glasshouses," *Journal of Wind Engineering and Industrial Aerodynamics*, vol. 6, pp. 139–187, 1980.
- [39] B. Bailey, A. Robertson, and A. Lockwood, "The influence of wind direction on greenhouse ventilation," *Acta Horticulturae*, vol. 26, no. 663, pp. 197–203, 2002.
- [40] J. Campen and G. Bot, "Determination of greenhouse-specific aspects of ventilation using three-dimensional computational fluid dynamics," *Biosystems Engineering*, vol. 84, no. 1, pp. 69–77, 2003. cited By (since 1996)73.



---

# Glossary

## List of Acronyms

<b>ABL</b>	Atmospheric Boundary Layer
<b>CFD</b>	Computational Fluid Dynamics
<b>DIC</b>	Diagonal Incomplete-Cholesky
<b>DNS</b>	Direct Numerical Simulation
<b>GAMG</b>	Generalized Geometric-Algebraic Multi-Grid
<b>GPL</b>	General Public License
<b>KKM</b>	Kasklimaat Model
<b>KNMI</b>	Koninklijk Nederlands Meteorologisch Instituut
<b>LES</b>	Large Eddy Simulation
<b>PBiCG</b>	Preconditioned bi-Conjugate Gradient
<b>PCG</b>	Preconditioned Conjugate Gradient
<b>PDEs</b>	Partial Differential Equations
<b>PISO</b>	Pressure Implicit with Splitting of Operators
<b>RANS</b>	Reynolds Averaged Navier-Stokes
<b>RNG</b>	Re-Normalization Group
<b>STL</b>	Stereolithography
<b>TNO</b>	Netherlands Organization for Applied Scientific Research
<b>VDI</b>	The Association of German Engineers

## List of Symbols

$\Gamma_\varphi$	Diffusion coefficient
$\varphi$	Transported quantity in non-dimensional form
$\Delta P_0$	Pressure distribution at ground level
$\Delta P_s$	Buoyancy pressure drop
$\Delta P_w$	Wind pressure drop
$\Delta T$	Temperature difference between inside and outside
$\rho$	Density
$\zeta$	Pressure drop coefficient
$C_p$	Pressure coefficient
$g'$	Reduced gravity
$h$	Reference height
$K$	Von Karman constant
$k$	Turbulent kinetic energy
$P$	Static pressure at some point in the flow
$P_0$	Static pressure at the undisturbed stream
$S_\varphi$	Source term
$U$	Velocity
$U$	Velocity
$U$	Velocity vector in the x direction
$u$	Wind speed
$u_*$	Friction velocity
$U_0$	Velocity of the undisturbed stream
$U_h$	Velocity at reference height
$V$	Velocity vector in the y direction
$W$	Velocity vector in the z direction
$z$	Vertical height
$z_0$	Surface roughness length
$C$	Constant
$h$	Measure of grid spacing
$p$	Order of convergence
$r$	Grid refinement ratio
$Ri$	Richardson number
$T$	Outside temperature